Signature page

Developing mineralogical and geochemical discrimination methods to classify Li-barren and Li-prospective pegmatites at the Chebogue lithium prospect, southwestern Nova Scotia, Canada

By
Yousef Yammine

A Thesis Submitted to
Saint Mary's University, Halifax, Nova Scotia
in Partial Fulfillment of the Requirements for
the Degree of Geology.

August 2024, Halifax, Nova Scotia

Approved: Jacob Hanley (supervisor)

Approved: Jarda Dostal (reader)

Approved: Adam Nissen (reader)

Date: August 15, 2024

Developing mineralogical and geochemical discrimination methods to classify Li-barren and Li-prospective pegmatites at the Chebogue lithium prospect, southwestern Nova Scotia, Canada

By
Youssef Yammine

A Thesis Submitted to
Saint Mary's University, Halifax, Nova Scotia
in Partial Fulfillment of the Requirements for
the Degree of Geology.

August 2024, Halifax, Nova Scotia

Approved: Jacob Hanley

Approved: Jarda Dostal

Approved: Adam Nissen

Date: August 15, 2024

Developing mineralogical and geochemical discrimination methods to classify Li-barren and Li-prospective pegmatites at the Chebogue lithium prospect, southwestern Nova Scotia, Canada

by Youssef Yammine

Abstract

The parental magma composition that produces a plutonic rock is what gives the lithium-bearing pegmatite its distinct elemental composition. Lithium, a sought-after incompatible element, is challenging to detect through most routine analytical techniques. It occurs in abundance commonly bonded within aluminosilicate minerals such as in spodumene ($LiAlSi_2O_6$).

This study focuses on comparing mineralogical, petrographic, and geochemical characteristics of the lithium bearing Brazil Lake pegmatite (BLP) with Li-barren pegmatitic float to identify correlations that may help identify unexposed Li endowments. The main objective is to investigate if the chemical composition and mineralogy of chemically-developed rocks can be used to differentiate between economic and sub-economic lithium rocks in the absence of spodumene. Thin section and SEM analysis identified major and accessory minerals to classify the samples of this study (Zone A, north of Brazil Lake). Whole-rock geochemical assay data was used to analyze trace element composition, and LA-ICP-MS analysis of spodumene and muscovite to compare the trace element concentrations of Zone A to LCT pegmatites in North America. Finally, muscovite fractionation modelling was conducted to discover the extent of fractionation of the samples and explore their origin.

Based on the Nb/Ta ratios from whole-rock assay data and the composition of the samples, Zone A pegmatites match the LCT classification suggested by Černý (1991). Pegmatites with high Li content also correspond to specific ranges in trace elements. The composition of Zone A spodumene is most similar to the BLP, suggesting a common source. This is further supported through muscovite fractionation modeling, which suggested a similar amount of fractionation, due to a low K/Rb ratio and high Cs concentration shown in Zone A and BLP.

Overall, this research intends to find a way to facilitate lithium detection and to more reliably uncover lithium prospective deposits.

[August 15, 2024]

Acknowledgements

I would firstly like to thank Dr. Jacob Hanley for his unlimited help and patience throughout this project. Thank you to Paul Smith, Steven Crowell and everyone else involved at CL-MC for giving me to opportunity to work on this project and providing the samples. A special thank you to Dr. James Brenan at Dalhousie University for taking time out of his day to help me with the LA-ICPMS analysis and Xiang Yang at Saint Mary's University for his unlimited help on the SEM. And finally, none of this would be possible without my friends for being a literal and metaphorical shoulder to lean on, and to my family for their infinite belief in me.

Table of Contents

List of Figures

List of Tables

1.0 Introduction

Lithium is the lowest density metallic element on the periodic table, with a high standard electrochemical potential, which makes it perfect as an anode material in rechargeable batteries (Kundu et al., 2022). Lithium is mainly found in granitic pegmatites, with spodumene ($LiAlSi_2O_6$) being the main mineral from which lithium is extracted, while lepidolite [K (Li, Al)$_3$(Al, Si, Rb)$_4$O$_{10}$(F, OH)$_2$] and petalite ($LiAlSi_4O_{10}$) also bear lithium in small percentages (Table 1). In addition Li brine deposits are currently the primary source of industrial lithium production (Steinmetz et al., 2018). Exploration for pegmatites presents several challenges, due to their variable mineral composition and relatively small deposit size with limited surface indicators. Canada's heightened interest in lithium stems from the gradual transition into clean energy, particularly renewable energy storage and electric vehicles. With Canada attempting to establish itself as a global supplier of critical minerals such as lithium, exploration for these resources is being intensified for domestic use and to meet the rising global demand (*The Canadian Critical Minerals Strategy, from Exploration to Recycling*, 2022).

Most classification schemes for pegmatites utilized in literature follow Černý (1991) for differentiating rare metal pegmatites such as LCT (lithium-cesium-tantalum), NYF (niobium-yttrium-fluorine), and mixed LCT and NYF. This classification system is based on the whole-rock composition of the pegmatite, associated granites and their bulk compositions, and the lithologies of the parental magma sources. There are various reasons why rare metal pegmatites are difficult to formalize in terms of a classification scheme. These features include their complex mineralogy, high concentrations of rare elements, differing grain sizes (often to extremes) and orientations resulting in complex textures (Wise et al., 2022). The mineralogy of each specific pegmatite family also varies greatly, in particular with respect to the diversity and complexity of accessory minerals. For this study, two main classification schemes were used in order to help classifying pegmatites: Černý (1991) and Wise et al. (2022).

Černý (1991) created a classification scheme that works well in differentiating the individual pegmatite through whole-rock geochemical characteristics but manages to abandon many pegmatites that are enriched in rare metals that fall outside of the classification scheme (Ercit, 2005). Černý & Ercit (2005) recognized textural features such as miarolitic cavities as important in the classification of a pegmatite into the REE class (Table A1). Miaroles are cavities

that form during the late stages of pegmatite formation at low pressure resulting from a confined volatile phase in the main pegmatite body that may escape during cooling and/or decompression depending on the tectonic conditions, leaving behind one or a number of crystal-lined pockets that once contained the saturated volatile phase (Candela, 1997). Černý & Ercit (2005) split the miarolitic class of pegmatites into two sub-classifications: MI-REE for pegmatites in which volatiles separated due to a sudden drop in pressure, and MI-Li for pegmatites in which the volatile phase separation occurred due to both a drop in pressure and the crystallization of minerals that may deplete the melt of specific elements such as lithium (Černý & Ercit, 2005).

A more recent method (Wise et al., 2022) classifies rare metal pegmatites in three separate groups, only using bulk mineralogy, along with accessory mineral assemblages. Wise et al. (2022), alternatively to Černý, do not use miarolitic cavities in specific group classifications. However, they use more macroscopic textural features to further classify pegmatites from the three groups into subdivisions: simple zoned, complex zoned, miarolitic and layered (Table A1) The three main groups are:

(i) Group 1 pegmatites can be separated into three subsections: beryl-phosphates, Li-rich with spodumene or lepidolite being the main Li indicator minerals, and Li-rich with petalite or elbaite as the main Li indicator minerals. Additionally, high P enrichment and cassiterite occurring along with Nb-Ta minerals (predominantly in highly fractionated pegmatites) are also indicators of Group 1 pegmatites.

(ii) Group 2 pegmatites, rich in quartz and microcline feldspar, but share major phases with Group 1, but differentiated by biotite being the dominant mica, along with fluorite and Fe-rich minerals such as magnetite and fayalite.

(iii) Group 3 pegmatites are also rich in quartz, K-feldspar, plagioclase, muscovite, biotite and garnet, but most importantly contain various assemblages comprising sillimanite, kyanite and andalusite.

This study focuses on boulder fields in the southwestern part of Nova Scotia, north and south of the Brazil Lake pegmatite (BLP) near the town of Yarmouth (Figure 1). The BLP and nearby boulder fields are being investigated by mining and exploration companies for their potential as Li resources for development in the near future. The boulder fields, comprising the Chebogue lithium project, are under investigation by Continental Lithium, a wholly owned subsidiary of Manhattan Corporation Limited (“CL-MC”). Much work has been done on the

BLP by D.J. Kontak (2003, 2005, 2006), D. Bradley (2016), and A. McCauley (2014). The BLP falls under the LCT classification as it is enriched in Li, Ta, Cs, and Rb; (Kontak, 2006), and was emplaced within an active shear zone, dated at ~366-395 Ma using U-Pb geochronology, during the Acadian Orogeny. The petrogenesis of the BLP led to it being referred to as an 'albite-spodumene pegmatite', since it defies conventional pegmatite formation patterns as they are relatively uniform bodies with little to no distinct intrusion-scale zonation, as seen in other pegmatites of this type, such as King's Mountain and Barroso-Alvão (Barros et.al, 2020).

The overall purpose of this study is to develop criteria to distinguish between lithium prospective and lithium barren pegmatites using geochemical mineralogical methods without having lithium bearing minerals directly present in the rock to observe in hand sample or thin section. The samples studied from the boulder fields north and south of the BLP lie in an area that is relatively poorly characterized with respect to pegmatites and related felsic magmatism, which makes analyzing and classifying them difficult. More specifically, the objective of this thesis is to predict the occurrence of lithium rich pegmatites in the absence of the main indicator mineral, spodumene, by finding a 'marker', whether it be a specific mineral suite, a whole-rock element composition ratio, and even the lack or presence of specific element enrichments. To accomplish this, whole rock geochemical analysis was conducted on all samples collected in the field, followed by thin section analysis on representative samples with variable Li content in order to discern the mineralogy and textural similarities and differences between each sample, and to provide information required for classification. Scanning electron microscope (SEM) analysis was used to examine the chemical composition of accessory minerals that are found in each sample.

Table 1: Typical Li contents in Li-bearing minerals (adapted from Labbé & Daw, 2012)

Li-Mineral	Ideal Formula	Class	Theoretical Li contents (wt. %)	Theoretical Li_2O contents (%)
spodumene	$LiAlSi_2O_6$	pyroxene group	3.73%	8.00%
petalite	$LiAlSi_4O_{10}$	feldspathoid group	2.27%	4.90%
eucryptite	$LiAlSiO_4$	phenakite group	5.51%	11.90%
bikitaite	$LiAlSi_2O_6.\ H_2O$	zeolite group	3.40%	7.30%
lepidolite	$KLi_2AlSi_3O_{10}(OH,F)_2$	mica group	3.84%	8.30%
zinnwaldite	$KLiFeAl_2Si_3O_{10}(F,OH)_2$	mica group	1.59%	3.40%
amblygonite	$LiAlPO_4(F,OH)$	amblygonite group	4.73%	10.20%
montebrasite	$(Li,Na)AlPO_4(OH,F)$	amblygonite group	1-4%	-
lithophilite	$LiMnPO_4$	triphylite group	4.43%	9.50%
triphylite	$LiFePO_4$	triphylite group	4.40%	9.50%
hectorite	$Na_{0.3}(Mg,Li)_3Si_4O_{10}(OH)_2$	smectite group	1.93%	4.10%
jadarite	$LiNaSiB_3O_7(OH)$	silicate group	2.85%	6.10%
zabuyelite	Li_2CO_3	lithium carbonate	18.79%	40.40%
elbaite	$Na(Li_{1.5}Al_{1.5})Al_6Si_6B_3O_{27}(OH)_4$	tourmaline group	1.11%	2.40%

2.0 Geological Setting

2.1 Regional Geology

The South Mountain Batholith is a peraluminous pluton located in the southwestern extent of the Appalachian Orogen, in the Meguma Terrane. As seen in Figure 1, the Meguma supergroup is divided into two metasedimentary subgroups dating from the Cambrian to Lower Ordovician (Waldron et. al., 2009), the primarily sandstone rich Goldenville Group, and the dominantly siltstone and shale Halifax group. These groups represent a substantial clastic turbiditic succession likely deposited in a rift setting along the Gondwanan margin (White, 2009) and are overlain discomfortably by the Rockville Notch Group.

The supercontinent Rodinia fully broke apart at ~600 Ma due to extension in a back-arc setting. The magmatism that occurred is hypothesized to be related to the opening of the Iapetus Ocean ~590 Ma (Swanson-Hysell, 2021) evolved through a complex network of rifts, and

separated three large masses of land, Gondwana, Baltica and Laurentia. By the Early Cambrian to Mid-Ordovician (~485-470 Ma), Iapetus began closing, converging these three large continents, leading to the creation of the Pangean supercontinent. Avalonia, a fragment of what once was Rodinia, was wedged in between Laurentia and Baltica, and was pushed through tectonic activity into the Laurentian side, contributing to the formation of Pangea through the Acadian Orogeny, generally believed to have occurred in Devonian times (Osberg et.al, 1989), which eventually led to the formation of the Acadian Mountain Belt and further uplift. After the deformation caused by the Acadian Orogeny, the South Mountain Batholith (SMB), a large composite igneous intrusion, was emplaced between 360-375 Ma (Bickerton et al., 2022). The SMB is dominated by granodiorite to monzogranite with some leucogranite units (MacDonald et al., 1992). Prior to and after the Acadian Orogeny, other orogenic events were the Taconic Orogeny during the Middle to Late Ordovician, and the Middle Permian Alleghenian Orogeny (DiPietro, 2013).

Following the breakup of Rodinia, the formation of an accretionary orogen during the Paleozoic began, and was completed after the three major orogenic episodes, and once the supercontinent completely formed (Hatcher Jr., 2010). The northern Appalachians evolved through the collision of two microcontinents of Avalon and Meguma. Meguma is the second largest terrane in the Canadian Appalachians and was the last of the major terranes to accrete against North America (Schenk, 1998). The Meguma supergroup is defined by thick turbiditic clastic successions deposited in a major rift setting along the Gondwanan margin and is divided into two groups: the Goldenville Group and the Halifax Group. The lower part of the Meguma Group, the Goldenville Group, formed in a shallow to deep marine setting through Cambrian sedimentation on the Gondwanan margin of the Iapetus and is defined by greywacke and feldspathic quartzite with pelitic interbeds (Kontak, 1998). The lower part, known as the Halifax Group, is dominated by a slate rich succession that evolved through the sedimentation of deep-sea muds in cold climates, in high latitudes of the Southern Hemisphere. Discomfortably overlying the Halifax Group is the White Rock formation (Rockville Notch Group), dominated by slate, quartzite and metavolcanic rocks (MacDonald et al., 2002), that may have formed through marine sands that were deposited under a cold, possibly glacial climate in the uppermost Ordovician to Silurian.

2.2 Local Geology

In the Meguma terrane, three pegmatite occurrences have been extensively studied: the ~395 Ma BLP LCT-type pegmatites (Kontak, 2006), the ~371 Ma Port Mouton beryllium rich NYF-type pegmatites (Currie et al., 1998) on the shore, southeast of the BLP, and the ~385 Ma Barrington Passage pluton south of BLP, containing biotite-rich granitic pegmatite dykes (Rogers et al., 1988). The most significant of these in terms of economic potential to date is the BLP, hosted in the Silurian shallow sedimentary rocks of the White Rock formation, located within the Rockville Notch group (Figure 1), which include quartzite, amphibole and pelitic schist (Brushett et.al, 2024), and overlies both Goldenville and Halifax Groups. The area was crosscut by many shear zones during the middle Carboniferous (White and Barr, 2017), into which the pegmatite melt was injected during a single extensional event; this is supported by the orientation of the pegmatite bodies, subvertical to the shear zone, and the size and shape of the quartz megacrysts, which have been fractured and subsequently occupied by grains of albite (Kontak, 2006). The pegmatite was weakly deformed and metamorphosed during the Acadian Orogeny and owing to its location in a high-grade shear zone environment, it is unlikely that it formed independent of magmatic activity in the area but is rather derived from a crustal granite at depth (Kontak, 2006). Kontak (2006) also describes zonation within the pegmatite, separating it into two stages, I and II, with stage I consisting of quartz, feldspar, muscovite and spodumene, and stage II dominated by albite, replacing K-feldspar.

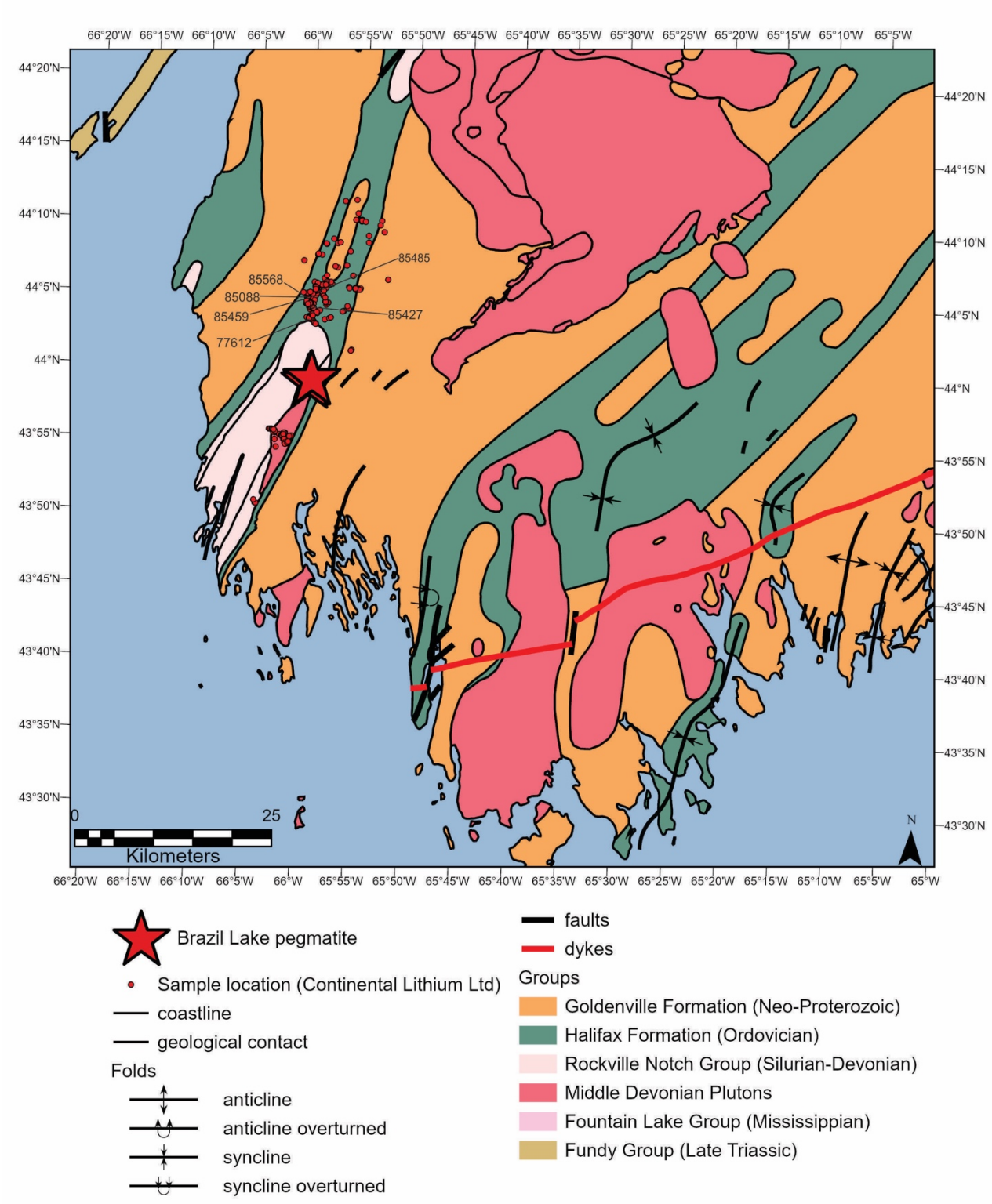

Figure 1: Simplified regional map of Southwestern Nova Scotia, including major rock groups found in the area. All bedrock geology and features gathered from Nova Scotia Department of Natural Resources and Renewables; all outcrop data supplied by CL-MC.

3.0 Methods

3.1 Sampling and Assay Methods

Samples were collected in the field by CL-MC from boulder trails north and south of BLP, with an originally much larger search area spanning from the bottom half of the SMB, south and west to the southern-most shore of Nova Scotia (Figure 1). Due to accessibility challenges, exploration was first initiated south of BLP (Zone B). However, once the northern claim block (Zone A) was identified as having a higher potential for Li discovery, all exploration attention was directed to that area (Steven Crowell, CL-MC geologist, personal communication, 2024). All assay data from the field was collected using the Fulcrum software. Samples were analyzed at Actlabs in Fredericton, New Brunswick, where ultratrace7- peroxide fusion ICP and ICP/MS analysis were used. The samples were fused with sodium peroxide (Na_2O_2) in a zirconium crucible and then acidified with concentrated nitric acid and hydrochloric acid. The resulting solutions were then diluted and measured by inductively coupled plasma optical emission spectroscopy (ICP/OES) and inductively coupled plasma mass spectrometry (ICP/MS). ICP/OES analysis from this lab have lower and upper detection limits for each element; if the sample analyzed contains less than the lower detection limit of lithium (>15ppm Li), then 8-Peroxide fusion is used. This assay method is useful for base metals, where a similar method was used as UT7, with samples once again fused with Na_2O_2, dissolved in purified water, and then acidified with concentrated nitric acid and hydrochloric acid. The sample is then measured with ICP-MS, with the lower detection limit this time being much lower by this method at 0.01% Li.

3.2 Thin Section Petrography and SEM Analysis

Initially, hand samples were provided by CL-MC for petrography analysis. They were subsequently cut and made into polished thin sections (27 mm × 46 mm, 30μm in thickness) at Saint Mary's University. These sections were studied under the Nikon Eclipse E400 petrographic microscope under transmitted light in order to identify and characterize minerals and textures present. The samples were then coated with carbon and analyzed under the scanning electron microscope (SEM), using back scattered electrons (BSE) in order to identify unknown grains, compositions of major and minor elements in large grains, as well as smaller, bright grains containing trace elements. The instrument used was a TESCAN MIRA 3 LMU field emission SEM. The EDS used is an Oxford Instrument X-Max 80mm^2 SDD energy dispersive spectrometer, using a High Voltage of 20.0 kV, with a working distance of 17-17.45 mm and an energy dispersive spectra (EDS) acquisition of 30 seconds for all samples. Quantification of spectra from an in-house standard albite yielded major and minor oxide concentrations within 5-10% (relative) of the expected compositions.

3.3 LA-ICP-MS

Laser ablation inductively-coupled mass spectrometry (LA-ICP-MS) was done on select spodumene and muscovite grains at Dalhousie University (Halifax, Nova Scotia) on 3 thin sections (85459, 85427, 85088) and one 1-inch puck containing four types of grains to be used for comparison of chemical composition of unknown samples to known localities: a spodumene grain from Brazil Lake, a muscovite grain from Brazil Lake, a spodumene grain from the Hugo pegmatite in Keystone (Nevada, USA) and a spodumene grain from the Plumbago Mountain pegmatite in Andover (Maine, USA). The instrument used is a 213 nm laser ablation system coupled to a Thermo iCAP Q quadrupole mass spectrometer and equipped with a single Helium Kinetic Energy Discrimination (He KED) cell. Before and after each sample, four standard pucks were analyzed using two NIST-610 silica glass trenches with an ablation diameter of 25 μm and a length of approximately 300 μm as a primary calibration standard, followed by BHVO-1 (Hawaiian Basalt powder) and BIR-1 (Iceland Basalt trench) used as secondary standards of the same size. The laser repetition rate was set to 20 Hz with an energy density of 5 J/cm^3; the measurements involved 20 seconds of background helium collection, followed by 4 passes on each trench totaling 80 seconds on the sample and 40 seconds of washout.

Muscovite and spodumene grains within the thin sections were analyzed in 10-16 measurement blocks per sample, consisting of trenches and pits with a diameter of 30 µm. Each sample on the puck was ablated with 10-12 pits measuring 60 µm in diameter. Data was then reduced on the Iolite 4.0 software, with internal standardization using the ideal Al weight percentage for spodumene (27.40 wt. %) and Al in muscovite based on the average composition from our SEM-EDS data (37.3 wt. %). The detection limits for the elements uses the Longerich et al. (1996) approach.

4.0 Results

4.1 Hand Sample and Thin Section Petrography

The sections below describe mineralogy, grain size, textures and modal abundances within the six hand samples and thin sections that were prepared from representative pegmatite boulder samples from Zone A. The abbreviations for common minerals seen and discussed in this study are summarized in Table 2 below:

Table 2: Mineral abbreviations

Abbreviation	Mineral
Aeg	aegirine
Ap	apatite
Bck	brockite
Clb	columbite
Cst	cassiterite
Goy	goyazite
Ilm	ilmenite
Kfs	K-feldspar
Mag	magnetite
Mnz	monazite
Ms	muscovite
Pl	plagioclase
Py	pyrite
Qz	quartz
Spd	spodumene
Ttl	tantalite
Zr	zircon

4.1.1 Sample 1: 85459

This sample is an albite-quartz tonalitic pegmatite, characterized in hand sample by very coarse-grained (1-2 cm) pegmatite float with small (1-2 mm) visible muscovite grains, quartz, and small patches of tantalite grains (5-8 mm) (Figure 2A). In this sample, the main minerals are quartz (45 vol%), muscovite (15%), plagioclase (35%), and a small amount of spodumene (~5%), which occurs mainly as fine-grained acicular crystals and less abundant subhedral tabular grains. In thin section, the muscovite grains are mostly equant and tabular with lengths ranging from 0.25-1.1 mm, with the largest phenocryst around 4 mm in length, and the smallest ones showed a euhedral to subhedral granular texture between quartz and plagioclase grains (Figure 3F). Figure 3 shows the main characteristics present in this sample. Muscovite occurs in euhedral 'books' (i.e., thick, equidimensional grains, rather than thin, elongated laths; Figure 3 A, B, C, D) and occasionally as more elongated grains (Figure 3D). Plagioclase grains show albite and polysynthetic twinning, with lathy and acicular grains in a sub-trachytic texture (plagioclase grains are mostly aligned, with some inconsistencies) (Figure 3E); the plagioclase growth is adcumulate (minimal to no space between plagioclase grains), and a length up to 1 mm. Plagioclase laths show a general alignment (Figure 3E) or finer grain intergrowth with quartz (Figure 3F).

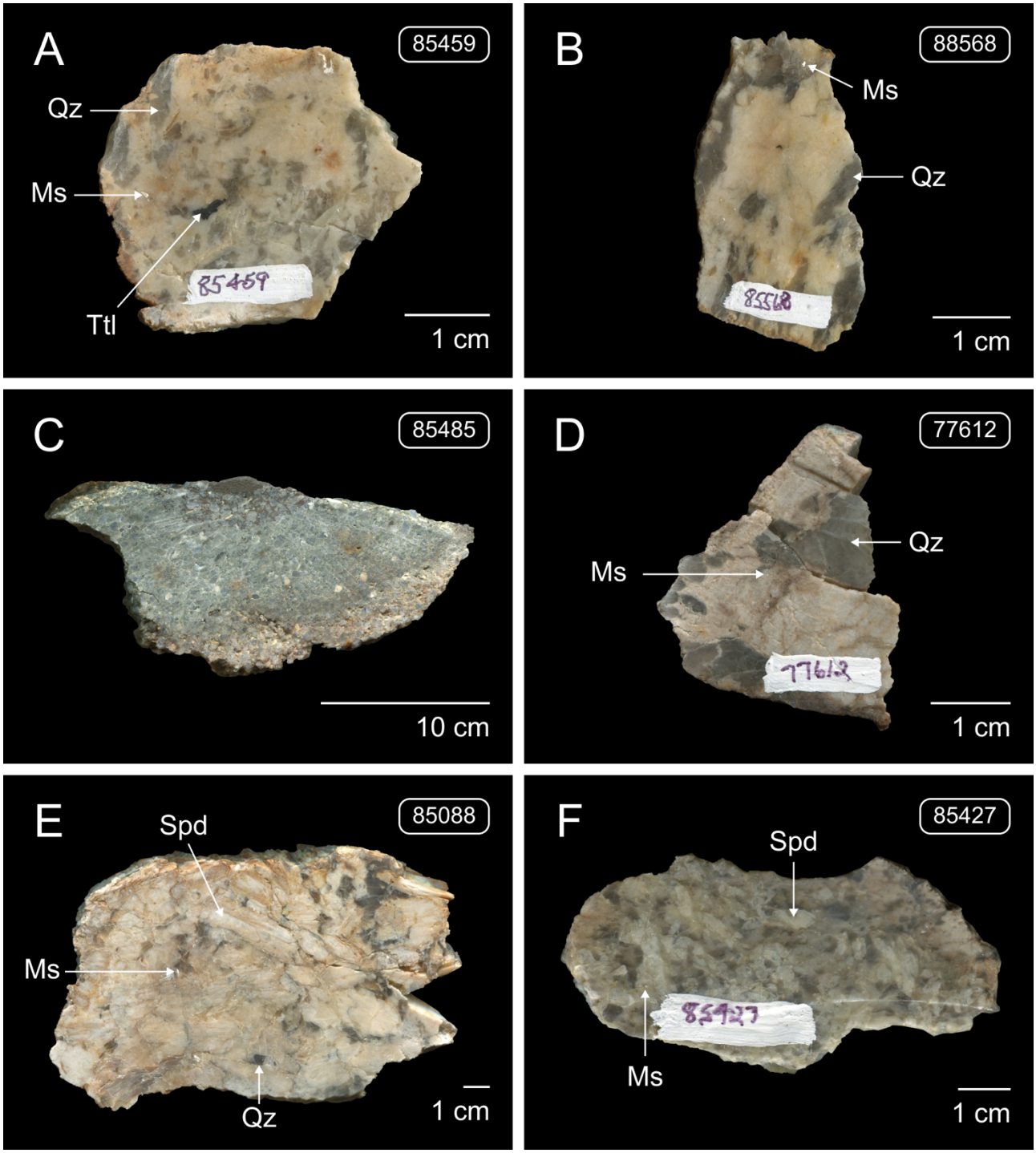

Figure 2: Cross sections of samples from Zone A (A) Figure 85459, a fine-grained tonalitic pegmatite showing predominantly quartz, muscovite along with visible tantalite (B) Albite-quartz-K-feldspar syeno-granite pegmatite, with subparallel quartz grains, feldspar and muscovite (C) Large coarse blue-grey metasandstone, likely from the Rockville Notch group, not a pegmatite (D) Small albite-quartz-K-feldspar syeno-granite with large well-formed quartz crystal and muscovite present in minimal amounts (E) Spodumene rich granitoid pegmatite with long spodumene laths with sub-parallel alignment occupying most of the sample, accompanied by quartz and muscovite (F) Spodumene rich syeno-granite pegmatite, with visible stubby spodumene grains floating in a fine-grained quartz-rich matrix, with small muscovite flakes visible.

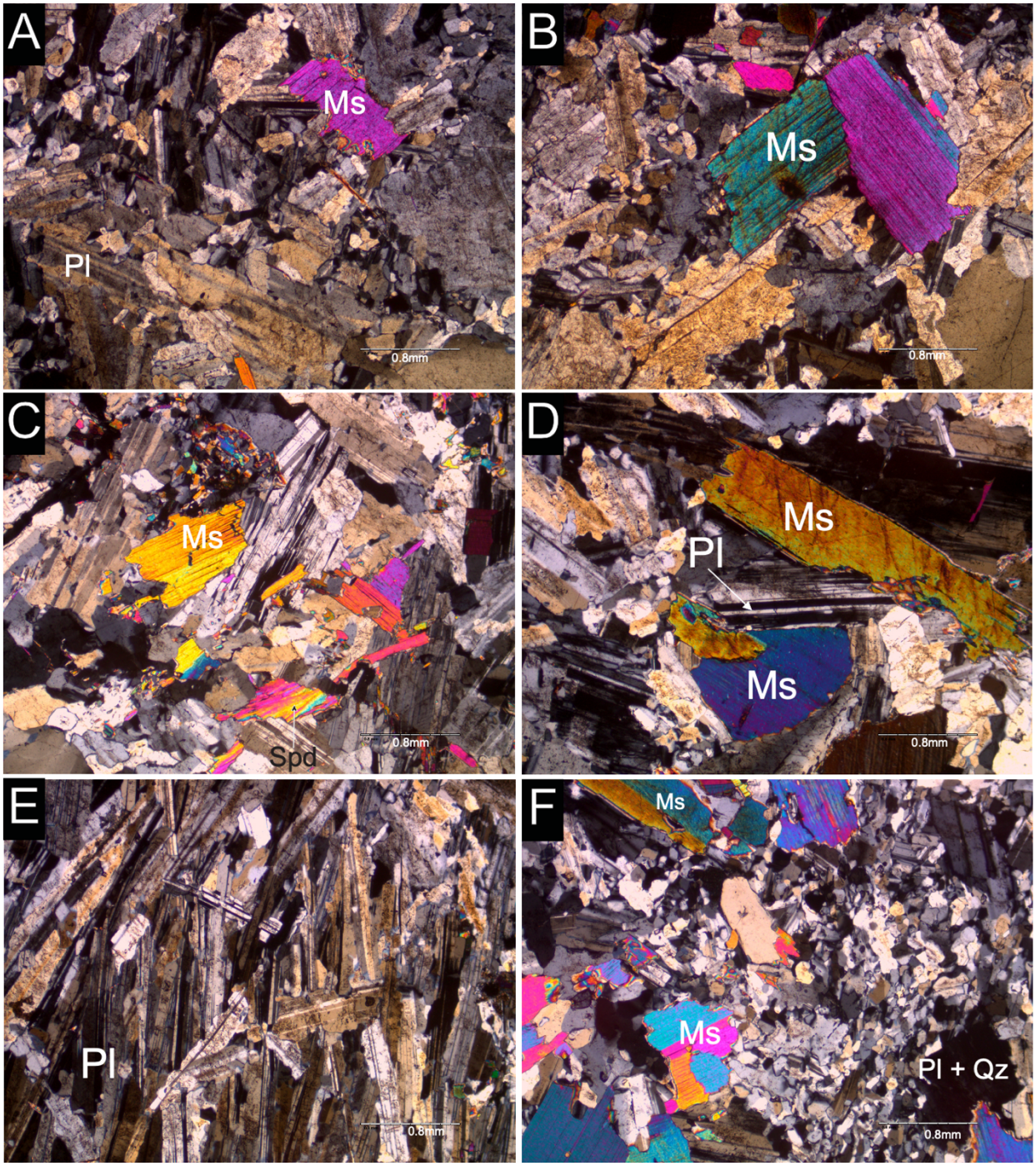

Figure 3: Thin section photomicrographs of various areas within sample 85459; (A) image of muscovite grain embedded within medium lathy plagioclase showing albite polysynthetic twinning (B) Two large muscovite grains oriented perpendicular to each other surrounded by plagioclase and quartz grains (C) Medium grained muscovite surrounded by plagioclase and spodumene (lower center right) (D) Lathy and subhedral muscovite aligned subparallel to the plagioclase grains (E) Large lathy and acicular plagioclase grains showing trachytic texture (F) Muscovite surrounded by smaller quartz grains with no well defined boundaries. All images in XPL, scale bar in bottom right represents 0.8 mm.

4.1.2 Sample 2: 85568

This sample is an albite-quartz-K-feldspar syeno-granite pegmatite, characterized by wide angular smoky quartz grains in albite, and containing small flakes of muscovite, with no spodumene grains visible to the naked eye (Figure 2B). The thin section is coarse to medium grained, with the majority of the surface area occupied by large euhedral, tabular potassium feldspar grains (55%) and quartz (20%). Figure 4 illustrates the characteristics of this sample, notably clusters of small (0.25-0.75 mm) lathy and euhedral muscovite (5%) grains within feldspars and between feldspar grains in veins (Figure 4 A, C). Plagioclase (15%) shows albite twinning in relatively large (~1-1.5 mm) grains, while platy acicular spodumene (<5%) occurs in a long vein between a large quartz and plagioclase grain (Figure 4B), with some spodumene evolving into a fibrous texture at the ends.

4.1.3 Sample 3: 85485

This hand sample is a sub-angular quartz-rich float (Figure 2C), while the cross section shows rounded to sub rounded small quartz grains (~5mm) intermixed with feldspar grains. The initial hand sample does not appear to be a pegmatite, but rather a coarse clast quartz-rich metasandstone, similar to what is seen in the Rockville Notch group (White & Barr, 2017). The thin section shows mostly coarse-grained rounded quartz (80%) with polygonal texture, and a trace amount of muscovite. The fine-grained matrix surrounding the grains seems to contain muscovite and other high interference coloured microcrysts that cannot be identified with regular microscopy, with opaques filling gaps between the quartz and the matrix. Figure 5 exhibits the textures seen in this sample, with fine-grained interlocking quartz (Figure 5A) and very small lathy muscovite grains (Figure 5C).

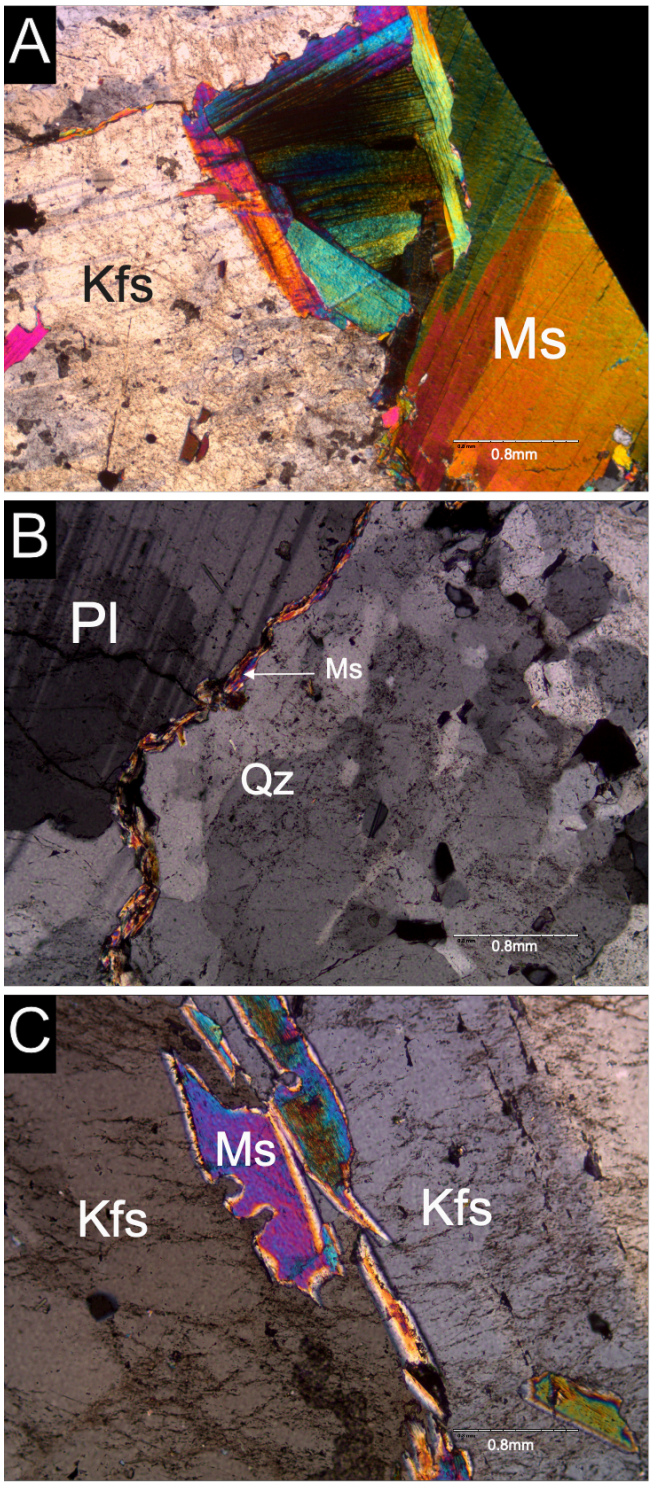

Figure 4: Thin section photomicrographs of Sample 85568 (A) Cluster of equant and tabular muscovite grains occurring on the edge of a large feldspar grain (B) Acicular muscovite and spodumene growing between large plagioclase grain showing albite twinning and quartz grain showing ondulose extinction (C) Tabular subhedral muscovite grains growing between feldspar grains. All images taken in XPL, scale bar in lower right corner represents 0.8 mm.

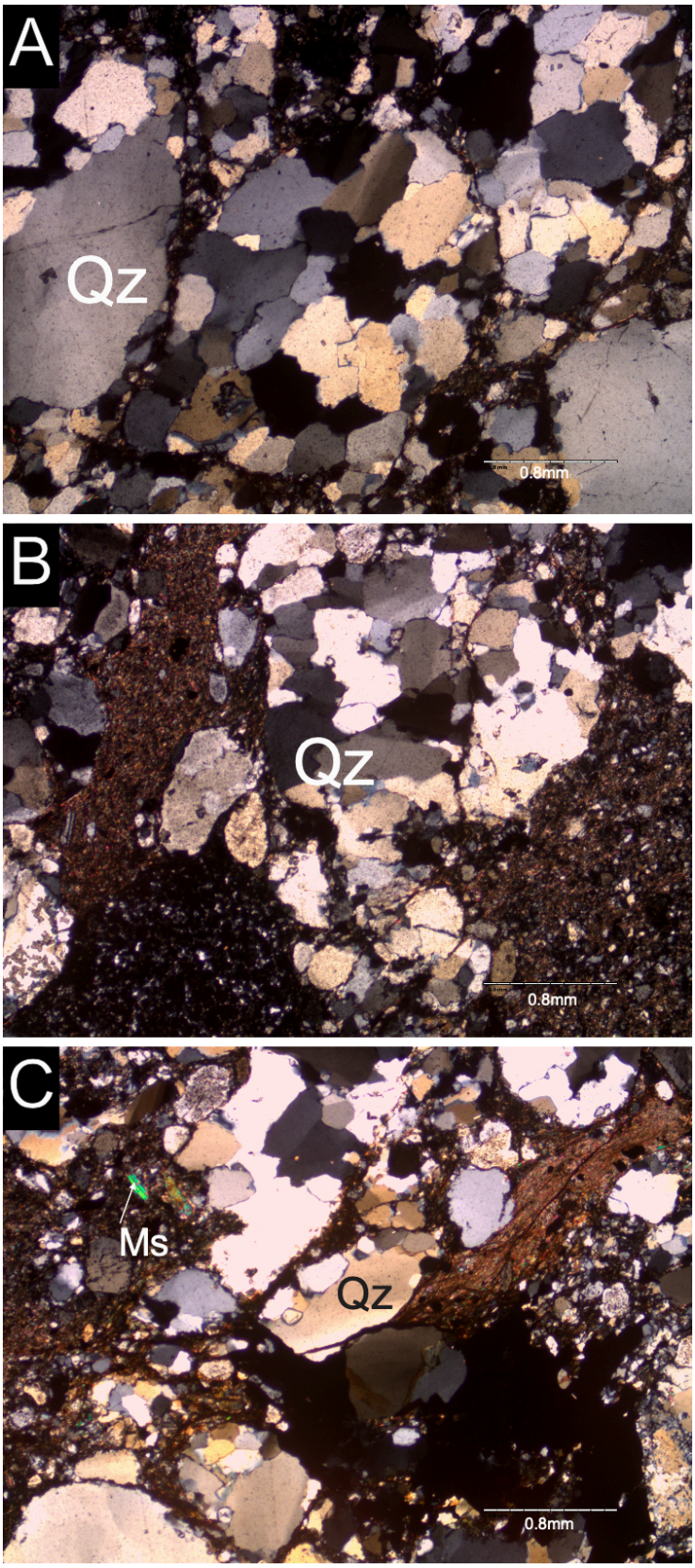

Figure 5: Thin section photomicrograph of Sample 85485 showing (A) equant to sub-equant quartz grains showing individual ondulose extinction (B) Quartz grains with no defined boundaries surrounded by fine grained ground mass on either side (C) Larger quartz grains with fibrous groundmass containing high interference color micas, and small muscovite grain on the left. All images in XPL, scale bar on bottom right represents 0.8 mm.

4.1.4 Sample 4: 77612

This sample, an albite-quartz-K-feldspar syeno-granite, shows mainly feldspar and subhedral smoky quartz grains, with a well-formed euhedral quartz crystal visible in the cross section, along with some small muscovite flakes (Figure 2D). Figure 6 shows the minerals and textures present in this sample; thin section showed very large quartz grains (35%) that can be seen by the naked eye (~2 cm in length), as well as early onset granoblastic texture (mosaic-like arrangement of small euhedral quartz grains, due to deformation and grain boundary migration), along with micrographic texture (fine intergrowth of quartz and K-feldspar). Lathy and tabular medium to fine-grained plagioclase (15%) only exhibit alignment in some parts of the sample (Figure 6D). Figure 6E shows long veins of acicular muscovite (~2.5%) and plumose (feather like pattern, radiating outwards) spodumene (~2.5%) radiating on the edges of large perthitic feldspar (45%) grains, and showing trachytic texture that seem to follow the edge of the phenocryst. Few large muscovite books were present in small concentrations, occurring within quartz and plagioclase grains (Figure 6D).

4.1.5 Sample 5: 85088

This sample is very spodumene rich with large visible lathy spodumene grains (3-4 cm) along with smoky quartz and muscovite; making it a spodumene rich quartz-plagioclase quartz-rich granitoid pegmatite (Figure 2E). Figure 7 shows very large coarse-grained subhedral and tabular spodumene grains (75%) that occupy the majority of the thin section (Figure 7 A, F), sometimes with simple twinning visible, and on some occasions occurring as acicular or fibrous. Fine-grained quartz (10%) and plagioclase (5%) showing a mosaic texture with no defined boundaries, along with small spodumene grains with no visible cleavage and second to third order interference colours can be seen in Figure 7E, with larger fine-grained tabular plagioclase grains showing albite twinning. Grains show no general orientation and muscovite (10%) occurs as tabular with the largest being around 1.3 mm, hosted within a large spodumene grain (Figure 7F), or as laths on the edges of one of the large spodumene grains (Figure 7A).

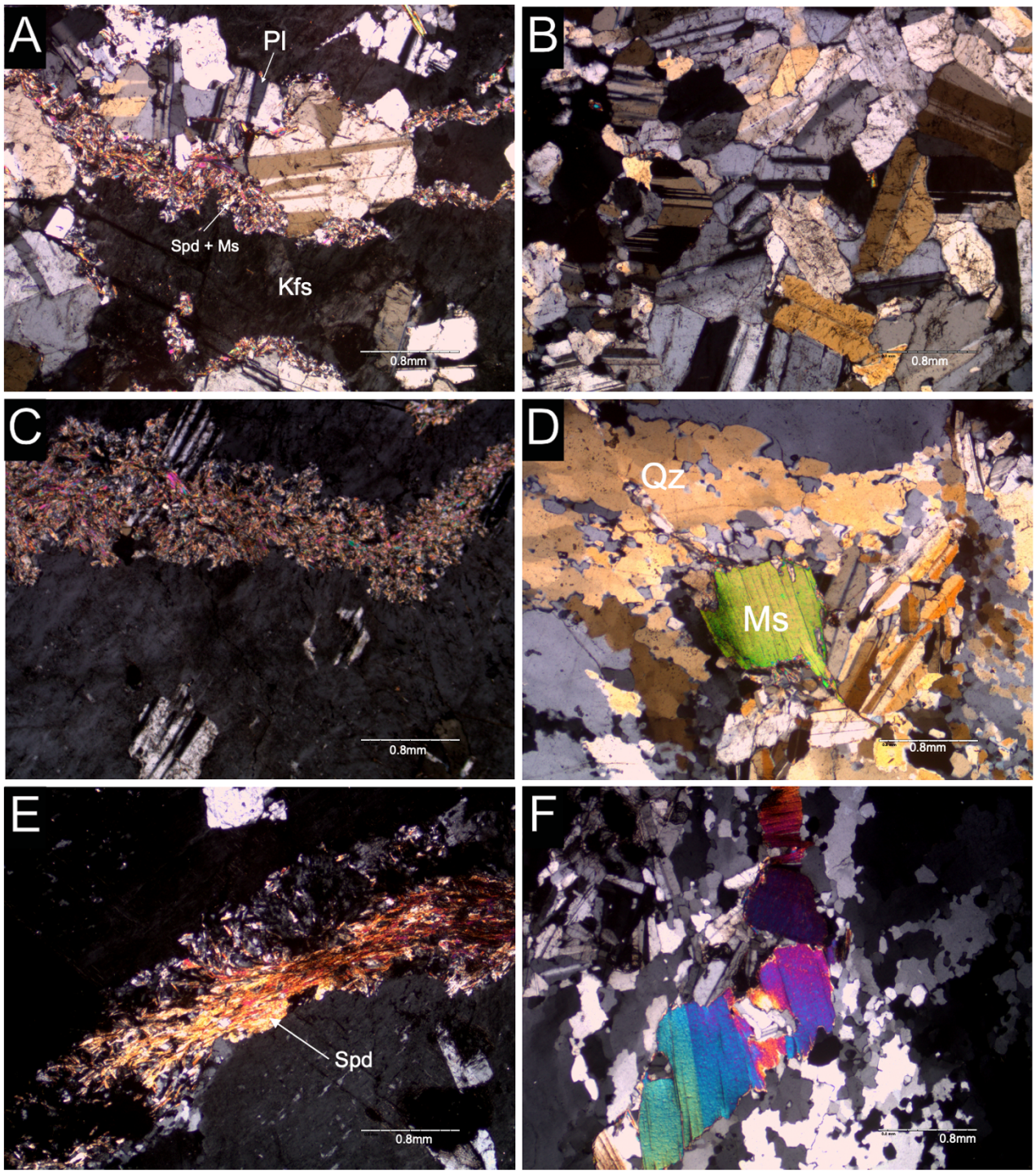

Figure 6: Thin section photomicrograph showing Sample 77612 (A) euhedral to subhedral tabular plagioclase grains showing twinning within large perthitic feldspar grain traced by acicular spodumene and muscovite vein (B) Tabular plagioclase veins showing simple and albite twinning with no specific orientation in an interlocking texture (C) Muscovite, spodumene and plagioclase acicular grains occurring in a vein between two large potassium feldspar grains (D) Euhedral muscovite grain surrounded by plagioclase laths oriented parallel to each other with large anhedral quartz grains with no defined grain boundaries (E) Plumose spodumene vein occurring between two potassium feldspar grains (F) Large subhedral muscovite books surrounded by granular quartz grains with onset granoblastic texture and plagioclase laths oriented subparallel to each other.

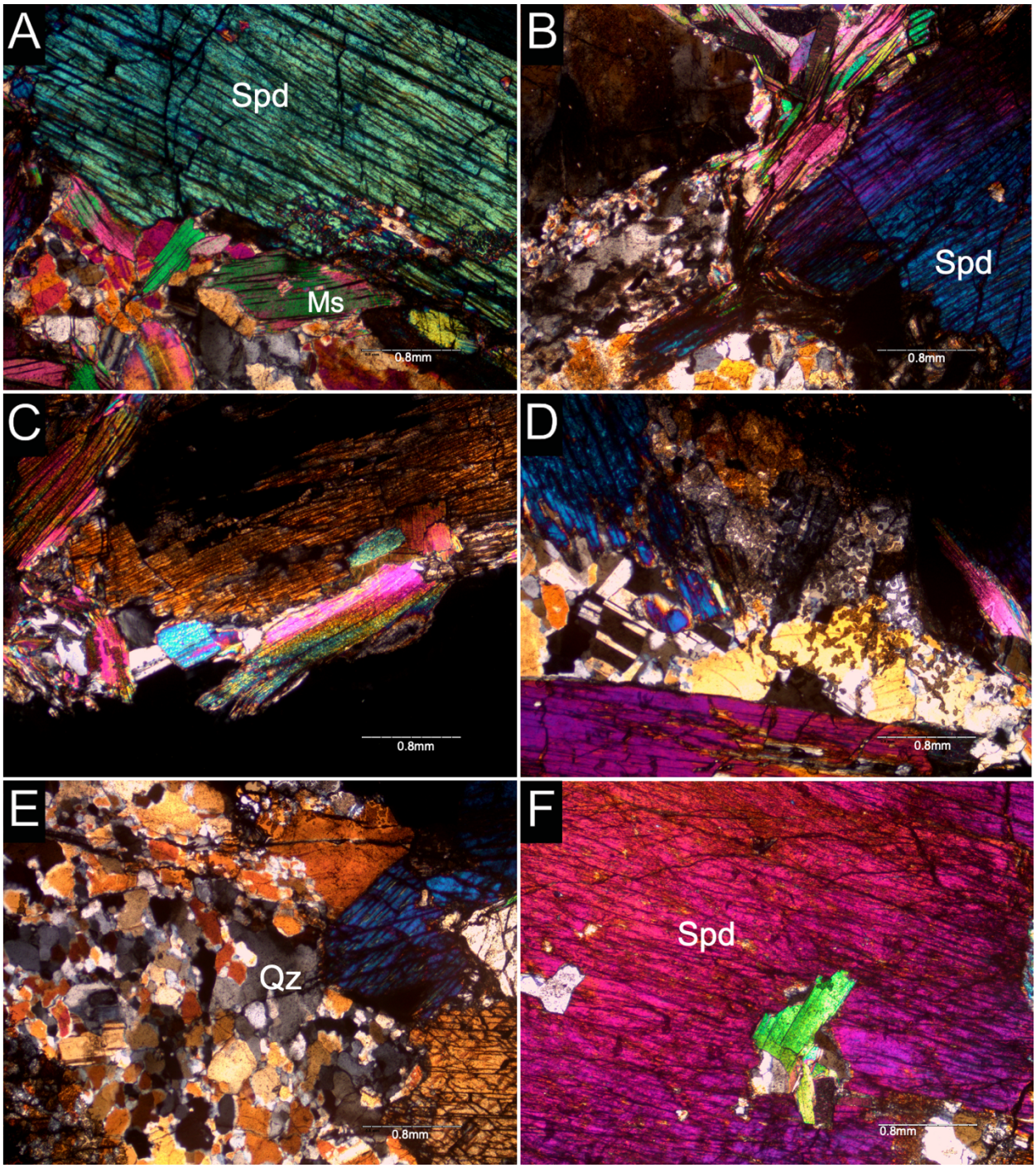

Figure 7: Thin section photomicrograph of Sample 85088 showing (A) very large spodumene grain with some alteration within bordering medium to fine grained subhedral muscovite grains (B) large tabular spodumene grain aligned subparallel to acicular muscovite grain towards anhedral quartz showing individual ondulose extinction (C) large spodumene grain aligned parallel to subhedral tabular muscovite grain below it (D) two large tabular spodumene grains aligned almost perpendicularly surrounding euhedral plagioclase grains and quartz (E) Rounded quartz grains with mostly no well defined boundaries bordering on two large spodumene grains (F) Subhedral tabular muscovite grain within very large spodumene grain which shows some alteration. All images in XPL, scale bar in bottom right corner represents 0.8mm.

4.1.6 Sample 6: 85427

This sample is classified as a spodumene-rich quartz-plagioclase-feldspar syeno-granite pegmatite. The hand sample is a large angular boulder, with common spodumene (40%) grains ranging from 0.5-2 cm floating in a fine-grained quartz-rich matrix, with K-feldspar (15%), quartz (20%) and muscovite (10%) sub-grains (Figure 2F). This sample showed one large tabular K-feldspar grain surrounded by medium-grained euhedral to subhedral muscovite. Figure 8 shows a large patch of around 4 mm in diameter, containing fibrous spodumene grains, all radiating inwards (Figure 8A), as well as large tabular spodumene (Figure 8 B, C). The spodumene grains seem to have a subparallel orientation, with some aligned perpendicular to the others. Microcrystalline quartz and plagioclase (5%) can be seen between spodumene grains, as can be seen in Figure 8C, while plagioclase shows simple, albite and microcline twinning surrounded by very fine quartz grains. Also present are subhedral, equant, altered unknown grains, with chevron type fractures and simple twinning, along with opaques that occupied ~10% of the thin section (Figure 8C).

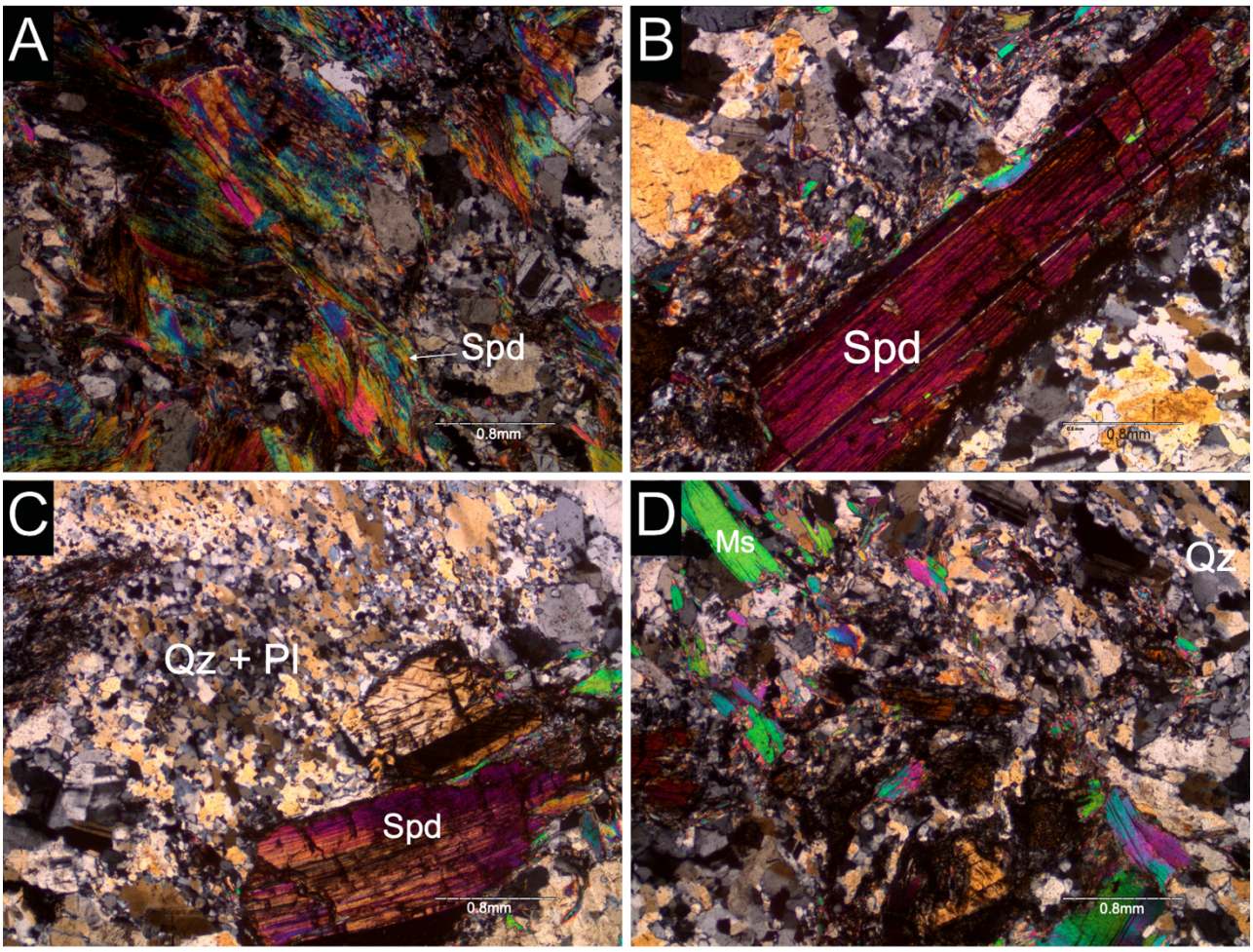

Figure 8: Thin section photomicrographs of Sample 85427 (A) Patch of plumose spodumene with no orientation surrounded by anhedral quartz and plagioclase grains (B) Large lathy spodumene grain with fine grained muscovite and plagioclase, as well as euhedral quartz grains surrounding it (C) Medium grained spodumene grain surrounded by intergranular quartz and plagioclase with no well defined grain boundaries (D) Muscovite grains with subparallel orientation within quartz. All images captured in XPL, scale bar in bottom right represents 0.8mm.

4.2 SEM-EDS analyses of feldspars and accessory phases

4.2.1 Feldspars

Feldspar compositions for 4 samples were determined by FE-SEM-EDS. From the 88 analyses, 53 plagioclase grains showed near pure albitic end-member, ranging from ~Ab_{97} to Ab_{100} composition, and 32 alkali feldspar showed near pure orthoclase end-member, ranging from ~Or_{94} to Or_{100} composition. Three grains of plagioclase were encountered showing anorthic composition (near An_{100}), and only a single alkali-feldspar showed an intermediate composition ($Ab_{56.03}$, $Or_{43.97}$). These analyses can be seen in Table A2.

Overall, almost all alkali feldspar grains analysed would plot on the outermost limb of an alkali feldspar binary system, which is inconsistent with the samples having magmatic origins, and suggests hydrothermal overprinting (Parsons, 1978), while the near pure end-member albite in this system likely stem from the albitization of plagioclase.

4.2.2 Accessory Minerals

The same method as section 4.2.1 was used to examine accessory minerals of interest in thin section, with the goal of identifying accessory phase composition as these are relevant to pegmatite classification (Table A3). The main accessory minerals encountered were apatite, cassiterite, columbite-tantalite, iron oxides, and rare phosphates such as goyazite [$SrAl_3(PO_4)(PO_3OH)(OH)_6$], as well as zircon. Four samples (77612, 85088, 85427, and 85459) exhibited a variety of accessory minerals, occurring in specific associations, as described below, with assemblages for all six samples seen in Table 3:

i. Phosphates: The strontium phosphate goyazite (Figure 9A) was found in sample 77612 along with iron oxides and aegirine ($NaFeSi_2O_6$). Goyazite occurs in cavities between large K-feldspar and albite grains (Figure 9A). Sample 85088 contained another rare phosphate, triphylite ($LiFePO_4$). Apatite [$Ca_5(PO_4)$], iron oxides such as hematite/magnetite, and ilmenite were seen in the samples, notably in sample 85485 (Figure 9D), where a large ilmenite grain can be seen in a fracture within the larger quartz grain, surrounded by smaller muscovite laths with no specific orientation; darker spots that are seen within this grain have a hematite/magnetite composition. Sample

85485 also shows small laths of chlorite accompanying muscovite surrounding the magnetite grain, which can be seen in Figure 9F. Sample 85459 exhibited the largest variation in accessory minerals, consisting mainly of apatite, columbite-tantalite, zircon, and monazite.

ii. Columbite-tantalite: Samples 85088 and 85427 contain columbite-tantalite group minerals, with 85427 showing both varieties of columbite (Mg-rich and Fe-rich). Columbite and tantalite occurred exclusively with each other displaying compositional zoning variations within the same grain, as can be seen in Figure 9C, with the brighter areas showing high Nb and low Ta, while the darker grey areas exhibited a substantially higher Ta concentration.

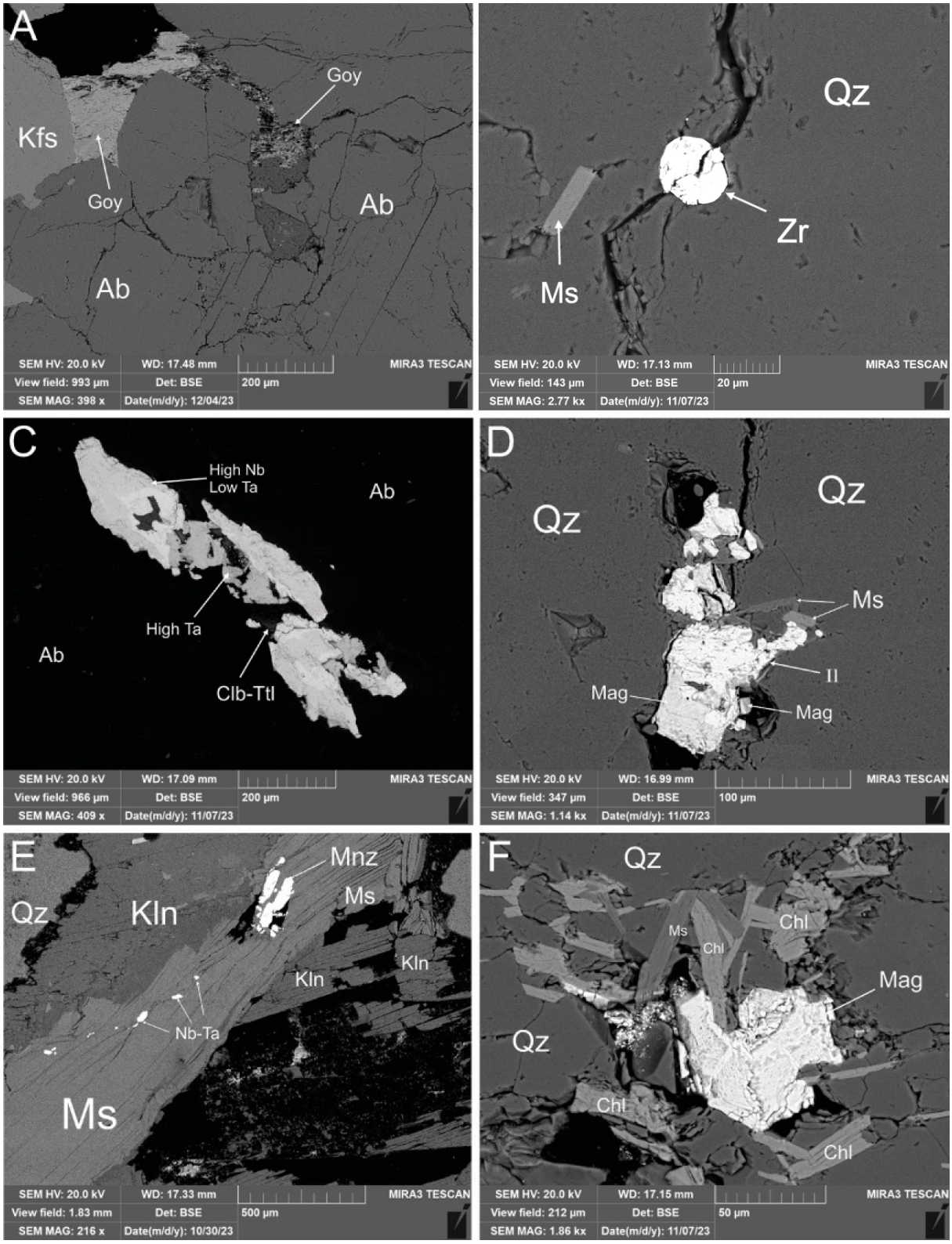

Figure 9: SEM photomicrographs of accessory minerals in various samples (A) Goyazite in sample 77612 occurring with quartz in a cavity between two large feldspar and albite grains (B) Zircon occurring in a fracture within a quartz grain along with muscovite in sample 85088 (C) Columbite tantalite grain showing variations in Ta and Nb concentrations in different zones in sample 85568 (D) Ilmenite grain with hematite and magnetite occurring within quartz along a fracture, showing variation in Ta, Mn and Ti concentrations in each section within the grain (E) Sample 85485 showing a large muscovite grain containing Nb-Ta grains as well as a large monazite grain, surrounded by kaolinite and quartz (F) Magnetite grain in quartz fracture surrounded by laths of chlorite and muscovite with subparallel orientation.

Table 3: Representative analyses of accessory minerals observed and identified by SEM

Sample	Aeg	Ap	Bck	Clb-Ttl	Cst	Goy	Ilm	Mag	Mnz	Zr	Tri
85459		x		xx					x	x	
85568				xx							
85485				xx			x	x			
77612	x			x-		x		x			
85088		x	x	xx	x						x
85427				x-	x					x	

4.3 Whole rock geochemistry of pegmatite and other felsic boulders

From the whole rock geochemistry assay data (Table A4) plots were made showing the relationship between bulk ppm concentrations and ratios of various trace elements against the concentrations of lithium in each sample to explore possible relationships. Data were separated into two sections or spatial domains, north (Zone A) and south (Zone B) of the BLP (Figure 1). Data for comparison from the BLP were obtained from Champlain Minerals Ltd. diamond drilling study in 2011 (Table A5). After review of all data, several interesting relationships were noted. First, the sample data were plotted showing Nb vs. Ta concentrations and the ratio of Nb to Ta concentrations. Lines of constant Nb/Ta ratio are shown on this plot (Figure 10A), as it is a very conservative ratio that cannot be influenced without extensive differentiation involving minerals that fractionate Nb strongly from Ta, or magma assimilation. Nb correlates to Ta forming 3 distinct trends showing ratios of: 100:1, 10:1, and 1:1 with a small amount of data falling on the 10:1 ratio line, while the majority laid between 10:1 and 1:1. Of the three groups plotted, it is worth noting BLP data and Zone A data mostly fall within the same region of the plot, between the 10:1 and 1:1 ratio lines, while Zone B data falls mostly on and around the 100:1 ratio line. Plotting Nb/Ta ratio against Li concentrations (Figure 10B), high Li concentrations (Zone A and BLP) correspond to relatively low ratios of Nb/Ta, ranging from 1 to 6. Similarly, high Li corresponds to low Mn and Sr concentrations, with Li in the 0.5-1 wt.% range, restricted to corresponding concentrations of 100-300 ppm and 10-20 ppm of Mn and Sr,

respectively (Figure 10 E, F). Similarly, high Li concentrations also correspond to a specific window of concentrations for other incompatible elements, including:

i. High Cs, ~10-100 ppm,
ii. High Rb, ~100-1000 ppm,
iii. High Sn, ~100-850 ppm,
iv. Low Ba, ~3-20 ppm,

(Figure 10 C, D, G, H), with all samples collected in Zone A corresponding strongly to the BLP data. For example, when Li concentrations in Zone A and BLP are greater than 1000 ppm, the Cs contents are always between ~10-100 ppm, however, when the Li concentration decreases, the Cs concentration can range between ~0.1-100 ppm (Figure 10C). In contrast, Zone B data did not extend into the higher Li window, but generally aligned with the concentration ranges observed in Zone A, with the exception of the Nb-Ta ratio, generally corresponding to the lower range in the ratio (Figure 10A).

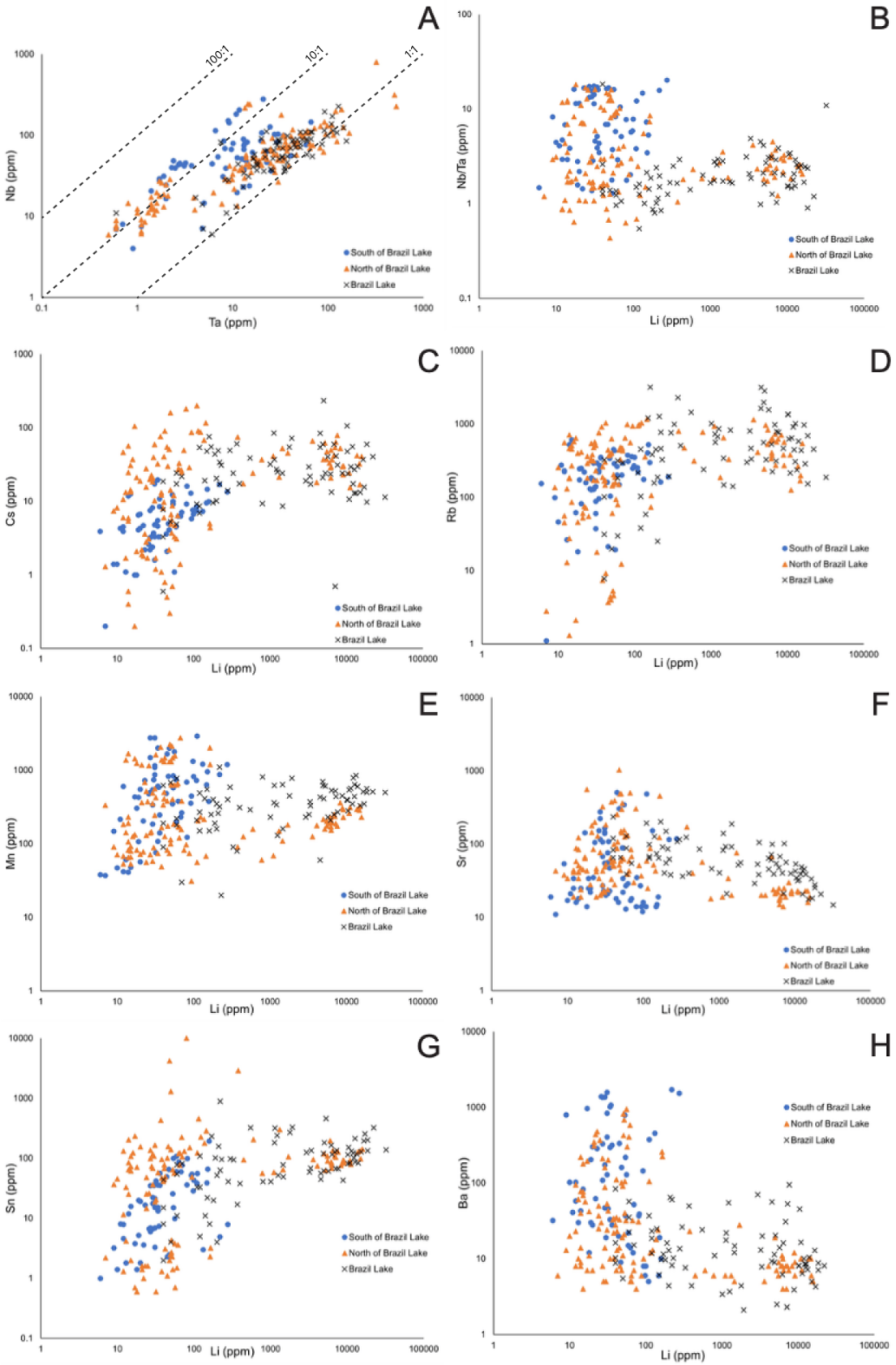

Figure 10: Scatter plot showing lithium concentrations (ppm) against various element concentrations (ppm) from whole rock geochemical assay data (A) Graph plotting concentrations of Ta against Nb (B) Li vs. Nb/Ta (C) Li vs. Cs (D) Li vs Rb (E) Li vs. Mn (F) Li vs. Sr (G) Li vs. Sn (H) Li vs. Ba. Assay Data for Brazil Lake was aquired from *Diamond drilling, prospecting & soil and gas hydrocarbon survey Brazil Lake property* report by Champlain Mineral Ventures LTD (2011).

4.4 LA-ICPMS analyses of spodumene and muscovite

4.4.1 Spodumene and muscovite chemistry comparison for Zone A pegmatite boulders and Brazil Lake

LA-ICP-MS analysis was conducted on muscovite and spodumene grains in three selected thin sections (85485, 85427, 85088) and a puck containing spodumene from various pegmatites, including Brazil Lake (Table A6). Muscovite grains from Zone A showed a very high concentration of rubidium, reaching upwards of 4000 ppm, much higher than the Brazil Lake muscovite grain, which showed concentrations similar to the range shown in the primary and secondary standards (355-400 ppm). Additional samples of spodumene from established LCT pegmatites were analyzed to determine whether Zone A spodumene has similar chemical characteristics to Brazil Lake and other North American pegmatites (Keystone, South Dakota, and Andover, Maine). Ca, Ga, Fe, Zn, Ti and U and can be seen in Figure 11 below:

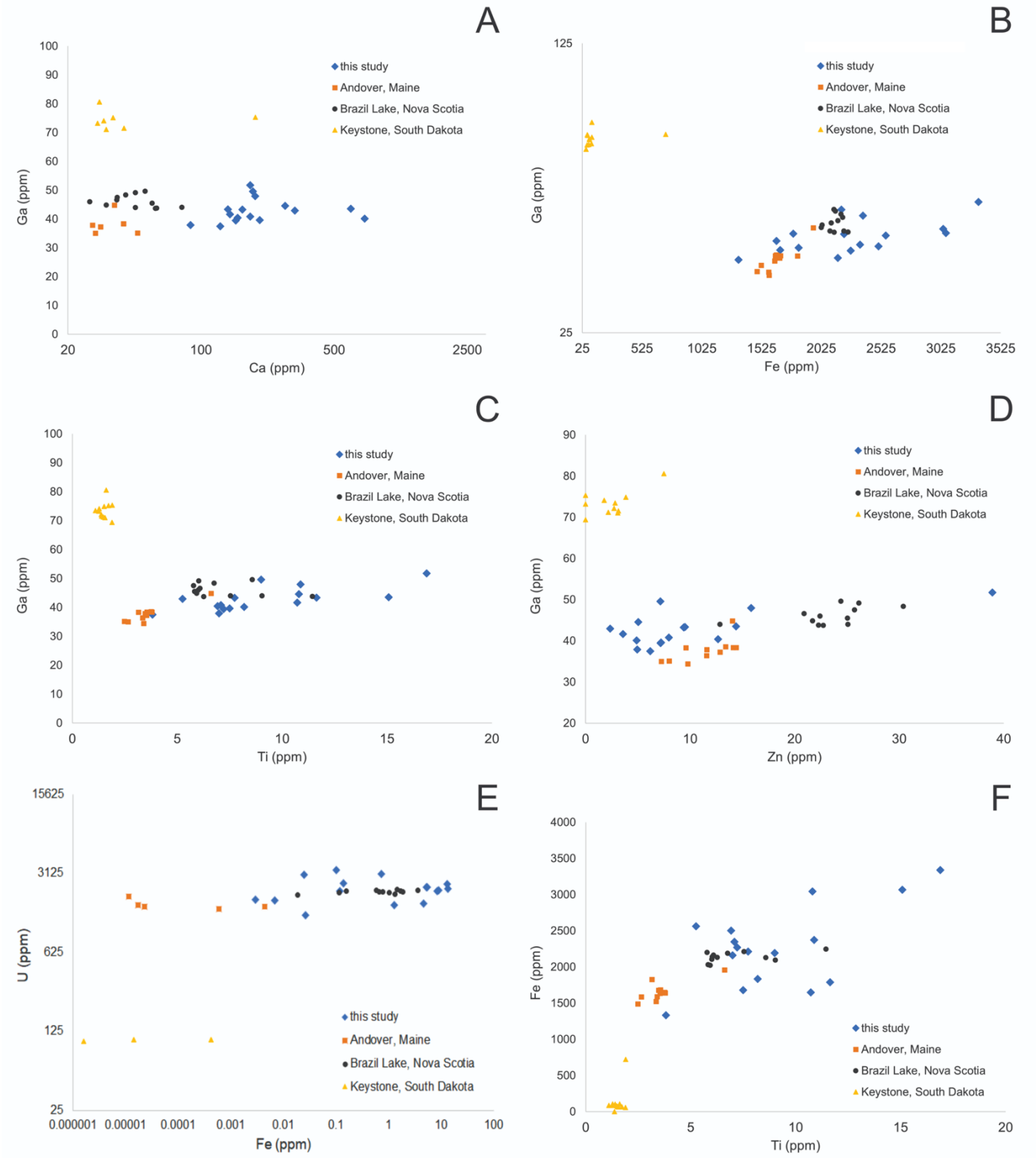

Figure 11: LA-ICP-MS graphs plotting concentrations of select elements from Zone A (this study) and other established LCT pegmatites in North America; (A) Concentrations of Ca vs. Ga, (B) Fe vs. Ga, (C) Ti vs. Ga, (D) Zn vs. Ga, (E) Fe vs. U, (F) Ti vs. Fe. All concentrations in ppm.

In these graphs, spodumene from Zone A has similar trace element compositions (Fe, Ga, Ti) to Brazil Lake and Andover, with the exception of Zn, where Brazil Lake shows a higher concentration than Zone A and Andover. Keystone, however, has very different trace element compositions to all three other sample sets, with significantly higher Ga concentrations, and lower Fe, Ti, and U concentrations.

4.4.1.1 Keystone, South Dakota

The Hugo pegmatite in Keystone, South Dakota described by Norton et al (1970) is characterized as an albite-quartz-perthite LCT pegmatite and with an age of 1.7 Ga (Orville, 1960). Figure 11 shows spodumene from Keystone as an outlier for all element concentrations relative to other LCT pegmatites and Zone A spodumene, with higher concentrations of Ga, ranging from 70-80 ppm, while Zone A, Brazil Lake and Andover ranged from 30-50 ppm. Keystone also exhibits much lower Ca than Zone A, Brazil Lake and Andover (~20-50 ppm compared to ~20-1000 ppm), low U and negligible Ti and Fe concentrations.

4.4.1.2 Andover, Maine

The Plumbago mountain pegmatite located in East Andover, Maine, formed during the Acadian orogeny and is dated between 288-297 Ma (Saltman, 2022). Samples from Andover match the trace element compositions of Zone A strongly for Ga, and Zn (respectively ~30-50 ppm and ~5-15 ppm), moderately for Fe, with an overlap window between ~1525-2025 ppm, and do not match for Ca, U and Ti.

5.0 Discussion

5.1 Classification of the Zone A pegmatite boulders

The Černý classification (1995) separates pegmatites into five subclasses based on mineralogical composition, metamorphic environment and structural features: abyssal, muscovite, muscovite rare element, rare earth element (REE) and miarolitic. The rare element subclass is divided into three petrogenic families: LCT, which also includes the miarolitic class, NYF and mixed. The LCT family is associated with granitic intrusions and contains Li, Rb, Cs, Be, Sn, Ta and Nb, with Ta > Nb, while NYF is marked by Nb, Ti, Y, Sc, Zr, U, Th and F, with Nb > Ta, and is associated with alkaline parental melts (Černý et al. 2005). Figure 10A was plotted with three Nb/Ta ratio lines, 100:1, 10:1, and 1:1, with the majority of data falling between the 10:1 and 1:1 ratio, which agrees with Černý's classification.

Another more recent system based on the 1995 classification was proposed by Wise et al. (2022), which provides a more systematic approach to classifying the pegmatites by using whole rock geochemical data and accessory minerals. This classification scheme separates pegmatites into three groups based on accessory and rock forming mineral assemblages. Group 1 is very similar to Cerny's LCT, containing beryl (with no Li, Nb, Ta), or an assemblage of spodumene, petalite and phosphates, and may contain biotite, muscovite and garnet. Group 2 is mainly composed of quartz and feldspar, but otherwise is very similar to Group 1 while it differs in some accessory minerals such as fluorite and magnetite and elevated Be. Group 3 is mainly composed of quartz, feldspar, plagioclase, muscovite and biotite, along with sillimanite, andalusite and kyanite. Biotite, muscovite, and columbite type minerals are present in all groups, but sample 77612 additionally contains aegirine, ilmenite and zirconium rich minerals, along with columbite, which match the group 2 classification, although the presence of spodumene overlaps with the group 1 classification. Samples 85088 and 85427 both contain columbite, apatite, as well as muscovite and spodumene, which corresponds to the group 1 classification. Sample 85459 notably contain zircon and apatite along with muscovite and spodumene, matching group 1. Sample 85485 contained a significantly higher amount of magnetite and ilmenite, along with muscovite, however, is not a pegmatite, as it is classified as a metasedimentary rock.

5.2 Comparison to Brazil Lake and other pegmatites

The samples from Zone A have a unique geochemical signature, however, they do share similar concentrations of trace elements to other established LCT pegmatites. As seen in Figure 11, the Zone A samples overlap mostly with Brazil Lake and with Andover, while the Hugo pegmatite in South Dakota is an outlier for concentrations of Ca, Fe, Ti, Zn, and U. Andover shares many general similarities with Zone A and Brazil Lake, possibly due to a similar mineralization and hydrothermal overprint (Landes, 1925), or due to metamorphism of a similar S or A type granitic melt, as these are the most likely to produce pegmatitic melts (Černý et al., 2012). Keystone is characterized by very high Ga, much lower Fe and Ti than the other LCT pegmatites studied, and slightly lower Zn. The pegmatite in Keystone shares similarities in composition to some of the samples, such as apatite, columbite, albite and cassiterite, but only in the intermediate zones of the pegmatite (Landes, 1928). The lower concentrations of Fe and Ti could be explained by these elements depleting from the granitic melt as it crystalizes, as their level tends to decrease as fractionation increases (London et al. 2020). The enrichment in Ga can be attributed to leucogranites as parental granites to rare earth element pegmatites (Černý et al.,1985).

Looking specifically at Zones A and B (north and south of Brazil Lake) in Figure 10, the high Li window Zone A corresponds closely with that of Brazil Lake. However, Zone A data displays a broad range of values, while Zone B exclusively overlaps with Zone A, and does not intersect the high Li window shared by Zone A and Brazil Lake.

5.3 Pegmatite origin based on modelled muscovite chemistry

The K/Rb ratio is considered to be a reliable indicator of the extent of compositional fractionation of the melt from which muscovite crystallizes and decreases with the progressive crystallization of a granitic magma due to the incompatible nature of Rb.

K/Rb decreases as the melt fractionates, so the ratio is lowest in most fractionated liquids. Cesium also increases rapidly during fractionation as it is strongly incompatible, and Cs-rich minerals only occur in the most extremely fractionated pegmatites. Rare metal pegmatites are often located near peraluminous granite plutons (Selway et al., 2005). Independent of their ability to generate pegmatites, fertile peraluminous granites have the potential to host economically significant concentrations of valuable minerals or ores (Černý, 1990).

A key question is whether pegmatites from which the Zone A boulders were sourced, and the BLP could have magmatic association with the SMB, a large peraluminous granitic batholith immediately west of the study area, or could have metamorphic origins related to the Acadian Orogeny. Ratios of K/Rb and Cs concentrations in magmatic muscovite grains from Zone A and Brazil Lake were compared to results of muscovite compositional evolution during batch crystallization. Modelling utilized various starting liquid compositions, including from the SMB, using melt inclusion data from Terekhova et al., 2023, in order to investigate if the pegmatites can be linked to the SMB. Partition coefficient data for Cs, Rb and K used in the modeling is from Icenhower and London (1995).

The initial composition depends on whether the samples are tied to a melt that is fractionated or not. The abundance of minerals controls the curvature of the graph while the top of the curve is dependent on the starting composition of the melt (Table 4). The changes in the graph are controlled by two factors: the Cs and K/Rb ratio present in muscovite, along with rock compositions; data for Brazil Lake was retrieved from Nissen et al. (2022). Different initial K, Cs and Rb concentrations in the melt have variable effects on the shape of the fractionation curve, as seen in figure 12; increasing the initial concentration of potassium has no effect, increasing the initial concentration of cesium reduces the slope of the curve, while increasing the initial rubidium concentration shifts the graph down along the y-axis. Additionally, percentages of common minerals such as albite, k-feldspar, quartz, spodumene and micas also have an effect on the fractionation curve; increasing the initial concentration of muscovite stretches the graph downward (Figure 12 C,D), while increasing biotite contracts the fractionation curve. Increasing albite percentages stretches the fractionation curve and moves it upwards, increasing the percentage of K-feldspar causes the graph to contract and shift up, while changes in quartz and spodumene percentages have no effect on the fractionation curve.

Table 4: Muscovite fractionation model for 3 scenarios: (1A**)** Fractionation curve of SMB from McKenzie et al. (1975) and initial melt compositions from Terekhova et al. (2023) (1B) Theoretical fractionation model to match fractionation curve to Zone A and Brazil Lake samples (Brazil Lake data retrieved from Nissen et al. (2022), (2A,2B) Scenario 2 showing the effects of only changing muscovite composition on fractionation curve (3A,3B) Scenario 3 showing the effects of changing Rb and Cs initial melt composition.

Figure 12 A		**Figure 12 B**	
Scenario 1A		**Scenario 1B**	
Rock composition (%) (McKenzie et al. 1975)		**Rock composition (%)**	
Albite	33	Albite	3
K-Feldspar	23	K-Feldspar	3
Quartz	32.1	Quartz	31.5
Spodumene	0.3	Spodumene	60
Muscovite	3.4	Muscovite	2.5
Biotite	8.2	Biotite	0
Starting melt composition (ppm) (Terekhova et al. 2023)		**Starting melt composition (ppm)**	
K	40000	K	40000
Rb	200	Rb	210
Cs	3	Cs	80

Figure 12 C		**Figure 12 D**	
Scenario 2A		**Scenario 2B**	
Albite	30	Albite	30
K-Feldspar	25	K-Feldspar	25
Quartz	30	Quartz	20
Spodumene	0	Spodumene	0
Muscovite	15	Muscovite	25
Biotite	0	Biotite	0
Starting melt composition (ppm) (Terekhova et al. 2023)		**Starting melt composition (ppm)**	
K	40000	K	40000
Rb	200	Rb	200
Cs	3	Cs	3

Figure 12 E		Figure 12F	
Scenario 3A		**Scenario 3B**	
Albite	30	Albite	30
K-Feldspar	25	K-Feldspar	25
Quartz	30	Quartz	20
Spodumene	0	Spodumene	0
Muscovite	15	Muscovite	25
Biotite	0	Biotite	0
Starting melt composition (ppm)		**Starting melt composition (ppm)**	
K	40000	K	40000
Rb	200	Rb	350
Cs	100	Cs	150

Table 4 and Figure 12 show three possible scenarios for muscovite fractionation, modelled in order to exhibit the extent of fractionation of Zone A samples. Table 4A and Figure 12A use the modal analyses of biotite granodiorites seen in McKenzie et al. (1975), which make up the bulk of the SMB, while the initial melt compositions were retrieved from Terekhova et al. (2023). Figure 12A shows the fractionation curve with all samples having a K/Rb ratio greater than 100, with very low Cs, while the Brazil Lake muscovite (Nissen et al, 2022) and the samples from Zone A contain a much lower ratio of potassium to rubidium and a higher concentration of Cs, showing a much more fractionated product. Scenarios 2A and 2B show the effect of increasing the percentage of muscovite, resulting in a more compressed fractionation curve, while scenarios 3A and 3B show the effect of increasing the earliest melt inclusions of Rb and Cs, resulting in a shift towards lower K/Rb ratio and stretches the fractionation curve towards a higher Cs concentration.

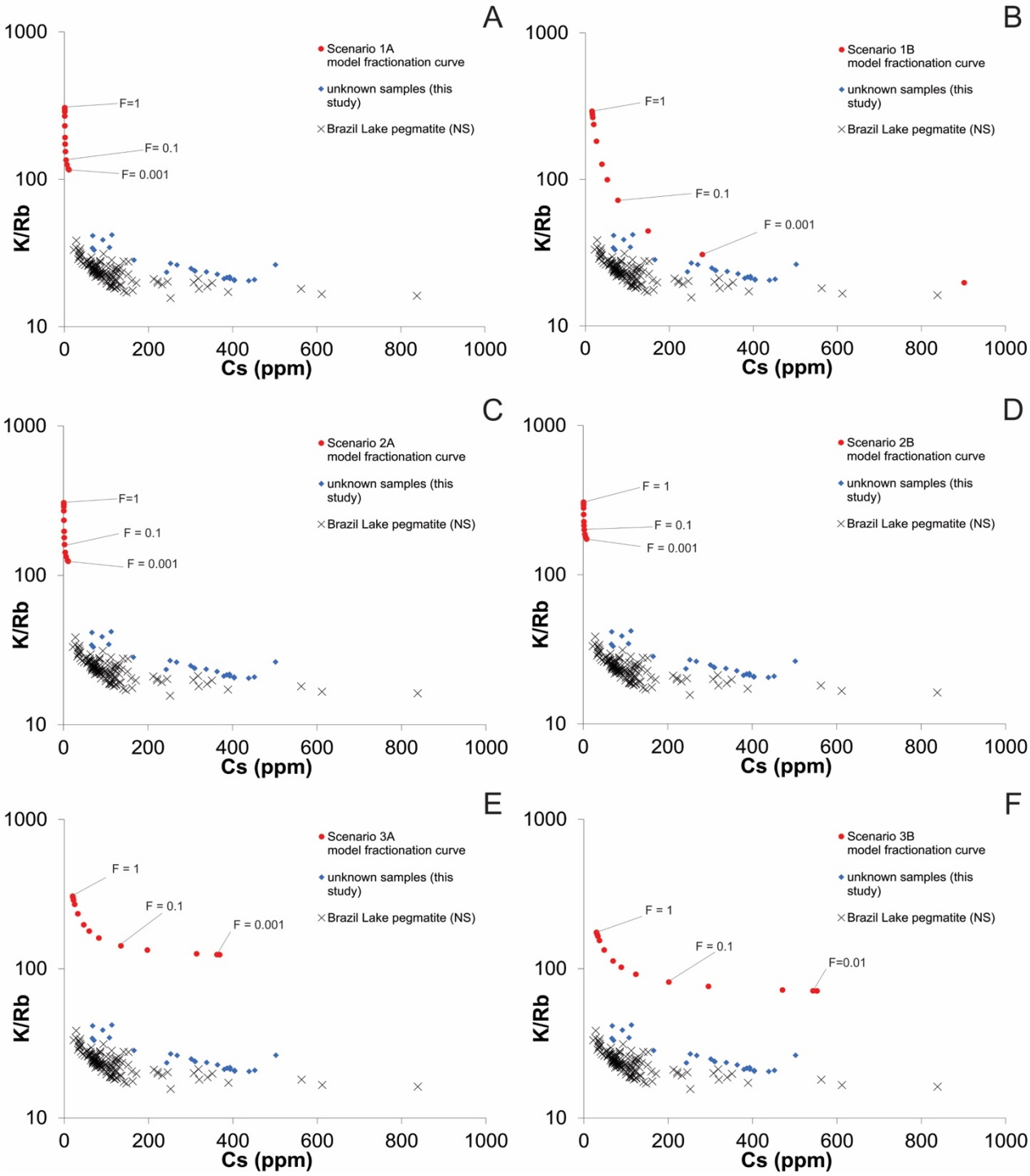

Figure 12: K-Rb and Cs muscovite fractionation curves showing three possible scenarios (A) South Mountain Batholith using modal analyses of the South Mountain Batholith from McKenzie et al. (1975) and initial melt compositions from Terekhova et al. (2023) (B) Model fractionation curve with composition and initial melt composition necessary for samples from the SMB to match Brazil Lake samples (Nissen et al. 2022) and the unknown samples from this study. (C, D) Scenario 2 showing the effects of increasing muscovite percentage (E,F) Scenario 3 showing the effects of increasing initial melt composition of Rb and Cs.

7.0 Conclusion

1. Pegmatite boulders from Zone A are consistent with the LCT pegmatite family classification, based on the enrichment trends they show in lithium, cesium and tantalum, as well as the high percentages of quartz and feldspar present in the samples, suggesting an S-type granitic composition. A low K/Rb ratio is also distinctive of LCT type pegmatites (London, 2008).
2. Whole rock geochemistry analysis shows that rocks from Zone A with a high Li content are only associated with a specific range in some trace elements:

- ~10-100 ppm Cs,
- ~100-1000 ppm Rb,
- ~100-1000 ppm Mn,
- ~10-80 ppm Sr,
- ~80-250 ppm Sn,
- ~2-10 ppm Ba.

Therefore, when analyzing Li-poor samples, any deviations from these expected ranges likely indicate that the samples are not associated with pegmatitic rocks containing spodumene that may be readily visible. Zone A pegmatites, that are Li-barren to Li-rich, share similarities with Brazil Lake in trace element ranges, unlike the barren Zone B pegmatites.

3. Spodumene chemistry shows that Zone A and the Brazil Lake pegmatite are similar, exhibiting a distinct spodumene compositional range, though are very different from other LCT pegmatites in North America, such as Keystone, South Dakota and Andover, Maine.
4. Muscovite composition modelling shows that in order to reach the extreme compositions of Zone A and the BLP, characterized by a low K/Rb ratio and high Cs concentrations, both these pegmatites would need to have undergone a similar amount of fractionation, have originated from the same parental melt, or a combination of both factors. The South Mountain batholith is an unlikely melt source as it is very weakly evolved and would require extensive fractionation in order to reach the melt composition required for the formation of these LCT pegmatites.

References

Archibald, D. B., Murphy, J. B., Reddy, S. M., Jourdan, F., Gillespie, J., & Glorie, S. (2018). Post-accretionary exhumation of the Meguma terrane relative to the Avalon terrane in the Canadian Appalachians. *Tectonophysics*, *747–748*, 343–356. https://doi.org/10.1016/j.tecto.2018.10.016

Barros, R., Kaeter, D., Menuge, J. F., & Škoda, R. (2020). Controls on chemical evolution and rare element enrichment in crystallising albite-spodumene pegmatite and wallrocks: Constraints from mineral chemistry. *Lithos*, *352–353*, 105289. https://doi.org/10.1016/j.lithos.2019.105289

Bickerton, L., Kontak, D. J., Murphy, J. B., Kellett, D. A., Samson, I. M., Marsh, J. H., Dunning, G., & Stern, R. (2022). The age and origin of the South Mountain Batholith (Nova Scotia, Canada) as constrained by zircon U–Pb geochronology, geochemistry, and O–Hf isotopes. *Canadian Journal of Earth Sciences*, *59*(7), 418–454. https://doi.org/10.1139/cjes-2021-0097

Bowell, R. J., Lagos, L., De Los Hoyos, C. R., & Declercq, J. (2020). Classification and Characteristics of Natural Lithium Resources. *Elements*, *16*(4), 259–264. https://doi.org/10.2138/gselements.16.4.259

Bradley, D. C., McCauley, A. D., & Stillings, L. M. (2017). *Mineral-Deposit Model for Lithium-CesiumTantalum Pegmatites* (Scientific Investigations Report) [Scientific Investigations Report].

Bradley, D., Shea, E., Buchwaldt, R., Bowring, S., Benowitz, J., O'Sullivan, P., & McCauley, A. (2016). Geochronology and Tectonic Context of Lithium-Cesium-Tantalum Pegmatites In the Appalachians. *The Canadian Mineralogist*, *54*(4), 945–969. https://doi.org/10.3749/canmin.1600035

Brushett, D. M., Beckett-Brown, C. E., McClenaghan, M. B., Paulen, R. C., Rice, J. M., Haji Egeh, A., & Pelchat, P. (2024). *Till geochemical data for the Brazil Lake pegmatite area, southwest Nova Scotia, Canada (NTS 21-A/04, 20-O/16 and 20-P/13): Samples collected in 2020, 2021, and 2022* (9148; p. 9148). https://doi.org/10.4095/332384

Candela, P. A. (1997). *A Review of Shallow, Ore-related Granites: Textures, Volatiles, and Ore Metals*. *38*(12).

Caporuscio, F. (2009). PEGMATITES by David London (2008).: The Canadian Mineralogist, Special Publication 10, 347 p. CDN$125.00 ($100.00 to members of MAC), ISBN: 978-0-921294-47-4. *American Mineralogist*, *94*(5–6), 862–862. https://doi.org/10.2138/am.2009.546

Černý, P. (n.d.). *Rare-element Granitic Pegmatites. Part I: Anatomy and Internal Evolution of Pegmatite Deposits*.

Cerny, P. (1991). *Rare-element granitic pegmatites. Part II: Regional to Global Environments and Petrogenesis*.

Černý, P., & Ercit, T. S. (1985). Some recent advances in the mineralogy and geochemistry of Nb and Ta in rare-element granitic pegmatites. *Bulletin de Minéralogie*, *108*(3), 499–532. https://doi.org/10.3406/bulmi.1985.7846

Cerny, P., & Ercit, T. S. (2005). THE CLASSIFICATION OF GRANITIC PEGMATITES REVISITED. *The Canadian Mineralogist*, *43*(6), 2005–2026. https://doi.org/10.2113/gscanmin.43.6.2005

Chakraborty, T., & Upadhyay, D. (2020). The geochemical differentiation of S-type pegmatites: Constraints from major–trace element and Li–B isotopic composition of muscovite and tourmaline. *Contributions to Mineralogy and Petrology*, *175*(7), 60. https://doi.org/10.1007/s00410-020-01697-x

Currie, K. L., Whalen, J. B., Davis, W. J., Longstaffe, F. J., & Cousens, B. L. (1998). Geochemical evolution of peraluminous plutons in southern Nova Scotia, Canada—A pegmatite-poor suite. *Lithos*, *44*(3–4), 117–140. https://doi.org/10.1016/S0024-4937(98)00051-6

Dessemond, C., Lajoie-Leroux, F., Soucy, G., Laroche, N., & Magnan, J.-F. (2019). Spodumene: The Lithium Market, Resources and Processes. *Minerals*, *9*(6), 334. https://doi.org/10.3390/min9060334

Diamond Drilling, Prospecting & Soil and Gas Hydrocarbon Survey Brazil Lake Property EL 05865 & EL 05866 (AR 2011-032; p. 489). (2011). Champlain Mineral Ventures LTD.

DiPietro, J. A. (2013). The Appalachian Orogenic Belt: An Example of Compressional Mountain Building. In *Landscape Evolution in the United States* (pp. 375–408). Elsevier. https://doi.org/10.1016/B978-0-12-397799-1.00023-3

Domeier, M. (2016). A plate tectonic scenario for the Iapetus and Rheic oceans. *Gondwana Research*, *36*, 275–295. https://doi.org/10.1016/j.gr.2015.08.003

Ercit, T. S. (n.d.). *REE-Enriched Granitic Pegmatites*.

Goodenough, K. M., Shaw, R. A., Smith, M., Estrade, G., Marqu, E., Bernard, C., & Nex, P. (2019). Economic mineralization in pegmatites: Comparing and contrasting NYF and LCT examples. *The Canadian Mineralogist*, *57*(5), 753–755. https://doi.org/10.3749/canmin.AB00013

Hatcher Jr., R. D. (2010). The Appalachian orogen: A brief summary. In *From Rodinia to Pangea: The Lithotectonic Record of the Appalachian Region* (p. 956). Geological Society of America.

Hellmann, R., Zhai, Y., Robin, E., Findling, N., Mayanna, S., Wirth, R., Schreiber, A., Cabié, M., Zeng, Q., Liu, S., & Liu, J. (2021). The hydrothermal alkaline alteration of potassium feldspar: A nanometer-scale investigation of the orthoclase interface. *Chemical Geology*, *569*, 120133. https://doi.org/10.1016/j.chemgeo.2021.120133

Home, R. J., MacDonald, M. A., Corey, M. C., & Ham, L. J. (1992). Structure and emplacement of the South Mountain Batholith, southwestern Nova Scotia. *Atlantic Geology*, *28*(1). https://doi.org/10.4138/1849

Keppie, J. D., Nance, R. D., Murphy, J. B., & Dostal, J. (1991). Northern Appalachians: Avalon and Meguma Terranes. In R. D. Dallmeyer & J. P. Lécorché (Eds.), *The West African Orogens and Circum-Atlantic Correlatives* (pp. 315–333). Springer Berlin Heidelberg. https://doi.org/10.1007/978-3-642-84153-8_14

Kesler, S. E., Gruber, P. W., Medina, P. A., Keoleian, G. A., Everson, M. P., & Wallington, T. J. (2012). Global lithium resources: Relative importance of pegmatite, brine and other deposits. *Ore Geology Reviews*, *48*, 55–69. https://doi.org/10.1016/j.oregeorev.2012.05.006

Kontak, D. J. (2003). *Geology of the Southern Lobe of the Brazil Lake LCT-type Pegmatite (NTS 21A/04), Yarmouth County, Nova Scotia*.

Kontak, D. J. (2006). NATURE AND ORIGIN OF AN LCT-SUITE PEGMATITE WITH LATE-STAGE SODIUM ENRICHMENT, BRAZIL LAKE, YARMOUTH COUNTY, NOVA SCOTIA. I. GEOLOGICAL SETTING AND PETROLOGY. *The Canadian Mineralogist*, *44*(3), 563–598. https://doi.org/10.2113/gscanmin.44.3.563

Kontak, D. J., Creaser, R. A., Heaman, L. M., & Archibald, D. A. (2005). U-Pb tantalite, Re-Os molybdenite, and 40Ar/39Ar muscovite dating of the Brazil Lake pegmatite, Nova Scotia: A possible shear-zone related origin for an LCT-type pegmatite. *Atlantic Geology*, *41*(1). https://doi.org/10.4138/655

Kundu, T., Rath, S. S., Das, S. K., Parhi, P. K., & Angadi, S. I. (2023). Recovery of lithium from spodumene-bearing pegmatites: A comprehensive review on geological reserves, beneficiation, and extraction. *Powder Technology*, *415*, 118142. https://doi.org/10.1016/j.powtec.2022.118142

Labbé, J.-F., & Daw, G. (2012). *Panorama 2011 du marché du lithium* (Public BRGM/RP-61340-FR; p. 155). la Compagnie Européenne d'Intelligence Stratégique (CEIS).

LaNlrs, Kbnn. K. (n.d.). *SEQUENCEOF MINERALIZATION IN THE KEYSTONE, SOUTH DAKOTA, PEGMATITES*.

London, D. (2014). A petrologic assessment of internal zonation in granitic pegmatites. *Lithos*, *184–187*, 74–104. https://doi.org/10.1016/j.lithos.2013.10.025

London, D. (2018). Ore-forming processes within granitic pegmatites. *Ore Geology Reviews*, *101*, 349–383. https://doi.org/10.1016/j.oregeorev.2018.04.020

London, D., Hunt, L. E., Schwing, C. R., & Guttery, B. M. (2020). Feldspar thermometry in pegmatites: Truth and consequences. *Contributions to Mineralogy and Petrology*, *175*(1), 8. https://doi.org/10.1007/s00410-019-1617-z

MacDonald, L. A., Barr, S. M., White, C. E., & Ketchum, J. W. (2002). Petrology, age, and tectonic setting of the White Rock Formation, Meguma terrane, Nova Scotia: Evidence for Silurian continental rifting. *Canadian Journal of Earth Sciences*, *39*(2), 259–277. https://doi.org/10.1139/e01-074

MacDonald, M. A., & Clarke, D. B. (2017). Occurrence, origin, and significance of melagranites in the South Mountain Batholith, Nova Scotia. *Canadian Journal of Earth Sciences*, *54*(7), 693–713. https://doi.org/10.1139/cjes-2016-0106

MacDonald, M. A., Home, R. J., Corey, M. C., & Ham, L. J. (1992). An overview of recent bedrock mapping and follow-up petrological studies of the South Mountain Batholith, southwestern Nova Scotia, Canada. *Atlantic Geology*, *28*(1). https://doi.org/10.4138/1848

Marchal, K. L., Simmons, W. B., Falster, A. U., Webber, K. L., & Roda-Robles, E. (2014). GEOCHEMISTRY, MINERALOGY, AND EVOLUTION OF Li-Al MICAS AND FELDSPARS FROM THE MOUNT MICA PEGMATITE, MAINE, USA. *The Canadian Mineralogist*, *52*(2), 221–233. https://doi.org/10.3749/canmin.52.2.221

McCauley, A., & Bradley, D. C. (2014). THE GLOBAL AGE DISTRIBUTION OF GRANITIC PEGMATITES. *The Canadian Mineralogist*, *52*(2), 183–190. https://doi.org/10.3749/canmin.52.2.183

McClenaghan, M. B., Brushett, D. M., Paulen, R. C., Beckett-Brown, C., Rice, J. M., Haji Egeh, A., & Nissen, A. (2023). *Critical metal indicator mineral studies of till samples collected around the Brazil Lake LCT pegmatite, southwest Nova Scotia* (8960; p. 8960). https://doi.org/10.4095/331537

Miall, A. D., & Blakey, R. C. (2008). Chapter 1 The Phanerozoic Tectonic and Sedimentary Evolution of North America. In *Sedimentary Basins of the World* (Vol. 5, pp. 1–29). Elsevier. https://doi.org/10.1016/S1874-5997(08)00001-4

Nissen, A., Kellett, D., Hanley, J.J., & Larson, K. (2024). Paired in situ 87Sr/86Sr and in situ 40Ar/39Ar mica geochronology of the Brazil Lake Li-Cs-Ta pegmatite. MSc. thesis, unpublished, Saint Mary's University

Norton, J. J., Page, L. R., & Brobst, D. A. (1962). *Geology of the Hugo Pegmatite Keystone, South Dakota* (Professional Paper) [Professional Paper].

Osberg, P. H., Tull, J. F., Robinson, P., Hon, R., & Butler, J. R. (1989). The Acadian Orogen. In *The Appalachian-Ouachita Orogen in the United States* (p. 782). Geological Society of America.

Parsons, I. (1978). Feldspars and fluids in cooling plutons. *Mineralogical Magazine*, *42*(321), 1–17. https://doi.org/10.1180/minmag.1978.042.321.01

Quéméneur, J., & Lagache, M. (1999). COMPARATIVE STUDY OF TWO PEGMATITIC FIELDS FROM MINAS GERAIS, BRAZIL, USING THE Rb AND Cs CONTENTS OF MICAS AND FELDSPARS. *Revista Brasileira de Geociências*, *29*(1), 27–32. https://doi.org/10.25249/0375-7536.1999292732

Rosing-Schow, N., Müller, A., & Friis, H. (2018). A Comparison of the Mica Geochemistry of the Pegmatite Fields in Southern Norway. *The Canadian Mineralogist*, *56*(4), 463–488. https://doi.org/10.3749/canmin.1700086

Rowe, R. B. (1954). Pegmatitic lithium deposits in Canada. *Economic Geology*, *49*(5), 501–515. https://doi.org/10.2113/gsecongeo.49.5.501

Roy, T., Plante, B., Benzaazoua, M., & Demers, I. (2023). Geochemistry and mineralogy of a spodumene-pegmatite lithium ore at various mineral beneficiation stages. *Minerals Engineering*, *202*, 108312. https://doi.org/10.1016/j.mineng.2023.108312

Saltman, E. J. (n.d.). *A Structural Analysis of the Plumbago Mountain Fault, Pluton, and Associated Pegmatites*.

Sánchez-Muñoz, L., Müller, A., Andrés, S. L., Martin, R. F., Modreski, P. J., & De Moura, O. J. M. (2017). The P–Fe diagram for K-feldspars: A preliminary approach in the discrimination of pegmatites. *Lithos*, *272–273*, 116–127. https://doi.org/10.1016/j.lithos.2016.10.030

Schenk, P. (1998). Sequence stratigraphy and provenance on Gondwana's margin: The Meguma Zone (Cambrian to Devonian) of Nova Scotia, Canada. *Journal of African Earth Sciences*, *26*(2), II. https://doi.org/10.1016/S0899-5362(97)83497-5

Selway, J. B. (2005). A Review of Rare-Element (Li-Cs-Ta) Pegmatite Exploration Techniques for the Superior Province, Canada, and Large Worldwide Tantalum Deposits. *Exploration and Mining Geology*, *14*(1–4), 1–30. https://doi.org/10.2113/gsemg.14.1-4.1

Shaw, R. A., Goodenough, K. M., Deady, E., Nex, P., Ruzvidzo, B., Rushton, J. C., & Mounteney, I. (2022). The Magmatic–Hydrothermal Transition in Lithium Pegmatites: Petrographic and Geochemical Characteristics of Pegmatites from the Kamativi Area, Zimbabwe. *The Canadian Mineralogist*, *60*(6), 957–987. https://doi.org/10.3749/canmin.2100032

Shellnutt, J. G., Owen, J. V., Yeh, M.-W., Dostal, J., & Nguyen, D. T. (2019). Long-lived association between Avalonia and the Meguma terrane deduced from zircon geochronology of metasedimentary granulites. *Scientific Reports*, *9*(1), 4065. https://doi.org/10.1038/s41598-019-40673-9

Steinmetz, R. Lucrecia López, et al. "Northern Puna Plateau-scale survey of Li brine-type deposits in the Andes of NW Argentina." Journal of Geochemical Exploration 190 (2018): 26-38.

Swanson-Hysell, N. L. (2021). The Precambrian paleogeography of Laurentia. In *Ancient Supercontinents and the Paleogeography of Earth* (pp. 109–153). Elsevier. https://doi.org/10.1016/B978-0-12-818533-9.00009-6

The Canadian critical minerals strategy, from exploration to recycling: Powering the green and digital economy for Canada and the world. (2022). Natural Resources Canada.

Tkachev, A. V., Rundqvist, D. V., & Vishnevskaya, N. A. (2018). Metallogeny of lithium through geological time. *Russian Journal of Earth Sciences*, *18*(6), 1–13. https://doi.org/10.2205/2018ES000635

Tollo, R. P., Bartholomew, M. J., Hibbard, J. P., & Karabinos, P. M. (2010). *From Rodinia to Pangea: The Lithotectonic Record of the Appalachian Region*. Geological Society of America.

van Staal, C. R., & Barr, S. M. (n.d.). *CHAPTER 2 LITHOSPHERIC ARCHITECTURE AND TECTONIC EVOLUTION OF THE CANADIAN APPALACHIANS AND ASSOCIATED ATLANTIC MARGIN*.

Waldron, J. W. F., White, C. E., Barr, S. M., Simonetti, A., & Heaman, L. M. (2009). Provenance of the Meguma terrane, Nova Scotia: Rifted margin of early Paleozoic Gondwana. *Canadian Journal of Earth Sciences*, *46*(1), 1–8. https://doi.org/10.1139/E09-004

White, C. E. (2010). Stratigraphy of the Lower Paleozoic Goldenville and Halifax groups in the western part of southern Nova Scotia. *Atlantic Geology*, *46*, 136–154. https://doi.org/10.4138/atlgeol.2010.008

Wise, M. A., Curry, A. C., & Harmon, R. S. (2024). Reevaluation of the K/Rb-Li Systematics in Muscovite as a Potential Exploration Tool for Identifying Li Mineralization in Granitic Pegmatites. *Minerals*, *14*(1), 117. https://doi.org/10.3390/min14010117

Wise, M. A., Müller, A., & Simmons, W. B. (2022). A proposed new mineralogical classification system for granitic pegmatites. *The Canadian Mineralogist*, *60*(2), 229–248. https://doi.org/10.3749/canmin.1800006